NTNU
Norwegian University of
Science and Technology

Buttresses on Flat-Slab Dams

Planning of Shear Tests

Andre' Nymo

Civil and Environmental Engineering
Submission date: June 2016
Supervisor: Leif Lia, IVM

Norwegian University of Science and Technology
Department of Hydraulic and Environmental Engineering

NTNU
Norges teknisk-naturvitenskapelige universitet

Fakultet for ingeniørvitenskap og teknologi
Institutt for konstruksjonsteknikk
Institutt for vann- og miljøteknikk

MASTEROPPGÅVE

Student: ANDRE NYMO

Tittel: PILARAR PÅ PLATEDAMMAR – PLANLEGGING AV TREKKEFORSØK

1 BAKGRUNN

Betongdammar skal vere både velte- og glidesikre. Det er framleis aktiv forsking på korleis heft, ruhet, friksjon, fortanning og boltar påverkar den reelle glidemotstanden mellom ein betongdam og fjellfundamentet. Vi står derfor i fare for å bygge og fornye konstruksjonar utan å kjenne den reelle kapasiteten mot gliding. Det kan føre til at konstruksjonar som anten ikkje er sikre nok eller til konstruksjonar som er unødvendig kostbart dimensjonert. For tida foregår det forskingsarbeid på temaet i samarbeid mellom NORUT (Narvik) og NTNU i prosjektet Stable Dams, på IFSTTAR (Lyon) i prosjektet CIBEFHY, på KTH (Stockholm) under leiing av Fredrik Johansson og på LTU i COMPLAB (Luleå). Det siste no er at Statkraft Region ØST planlegg å utføre fullskala forsøk med inntil fire pilarar frå ein platedam. Eit felt/fullskalaforsøk på platedampilarar vil tilføre forskingsmiljøet svært mykje informasjon, sidan dei nemnte prosjekta berre har utført testar og forsøk i laboratorie- og numerisk modell.

Platedampilarar har laster ifrå vasstrykk, istrykk og eigenlast. Det spesielle med slike pilarar er svært lita eigenlast i høve til på meir massive betongdamtyper. Det gjer at friksjonsleddet i ei stabilitetsberekning ($F_F = F_N \cdot \tan \varphi$) vert lite og pilarane vert sensitive for bidraget ifrå

kohesjon/heft. Det er berre testing i full skala med betongkonstruksjonar som har vorte påkjend med normale laster som vil gje rett svar på kor stort bidraget ifrå heft/kohesjon. Ulempa er at det ikkje vert mogeleg å skilje heft og kohesjon/ruhet ifrå kvarandre.

Arbeidet med masteroppgåva vil bli ein del av forsøksarbeidet til Statkraft, og er avhengig av dette for å kunne gjennomførast.

2 HOVUDPUNKT I OPPGÅVA

Arbeidet med prosjektoppgåva vil innehalde følgjande hovupunkt:

- Overordna planlegging av trekkeforsøk saman med Statkraft
- Grundig gjennomgang av alternative metodar for kapasitetsberekning
- Utveljing av pilarar på platedam i Telemark
    - Kartlegging av ruhet, geologi, helling, andre eigenskaper
- Bruke kjende metodar og berekningsgrunnlag for å finne forventa kapasitet
    - Handrekning (Patton, NTNU, Barton)
    - Avanserte metodar som FEM, evt Johansson
- Planlegging og eventuell gjennomføring av forsøk saman med Statkraft.
- Evaluering av resultat
- Rapportering

Innhaldet i prosjektet vil bli nærare avgjort av rettleiarane på basis av informasjon som kjem fram etter kvart som arbeidet går framover.

3 RETTLEIING, DATA OG INFORMASJON

Rettleiar vil vere Professor Leif Lia og medrettleiar blir siv.ing. Harald Andreas Simonsen i Statkraft. Andre naturlege diskusjonspartnerar er Fjola Gudrun Sigtryggsdottir på IVM og Eivind Grøv og Krishna Panthi på IGB.

Diskusjon med og bidrag frå andre medarbeidarar og studentkollegaer på NTNU, NORUT, SINTEF, NVE, Statkraft og andre kraftselskap vert tilrådd. Bidrag som går inn i oppgåva skal alltid refererast til på rett vis.

4 RAPPORTFORMAT, REFERANSAR OG ERKLÆRING

Oppgåva skal skrivast i eit tekstbehandlingsprogram slik at figurar, tabellar, foto osb. får god rapportkvalitet. Rapporten skal innehalde eit samandrag, ei innhaldsliste, ei liste over figurer og tabellar, ei litteraturliste og opplysningar om andre relevante referansar og kjelder. Oppgåva skal leverast i B5-format som .pdf i DAIM og trykkast i tre eksemplar som sendast direkte frå trykkeri til faglærer/institutt. Samandraget skal ikkje gå over meir enn 450 ord og skal vere eigna for elektronisk rapportering.

Masteroppgåva skal ikkje leverast seinare enn den leveringsfristen som kjem fram i DAIM (20 veker + offentlege fridagar vårsemesteret).

Trondheim, 8. januar 2016

_____

Leif Lia

Professor

d

e

Abstract

The shear strength of a bonded concrete-rock interface below a concrete dam consists of two parts: friction from the self-weight of the dam and cohesion due to the glue in the cement paste binding the surfaces together. For flat-slab buttress dams with low self-weight, the cohesive strength becomes extra significant for the sliding resistance. However, the Norwegian authorities on dam safety does not allow the use of cohesion in sliding stability calculations, unless the cohesive strength can be documented through tests. Yet, no proposal is given on how such tests should be carried out.

Consequently, the main scope of this thesis have been to develop and propose a test methodology to estimate the cohesive strength of Norwegian flat-slab buttress dams. The proposed testing procedure uses rock samples from the dam site to get the occurring roughness and strength of the bedrock. Furthermore, the test-specimen are prepared and concrete replicating the concrete of the dam are then cast on the natural surfaces of the rock samples. A series of shear tests is then carried out to measure the shear strength of the concrete-rock interfaces. Finally, the value of the cohesion is extrapolated out of the τ-σ curve. Preliminary testing of the methodology revealed the importance of thorough preparation of the test-specimen beforehand, but in the end left the author optimistic regarding the test methodology's future use.

Additionally, to investigate the effect of including cohesion in sliding stability calculations, the sliding safety of one of Statkrafts flat-slab buttress dams, Kalhovd dam, was assessed with a combination of FE-analysis and simplified hand calculations. The results showed that by assuming reasonable values for the cohesion, the dam managed to meet the requirements from the Norwegian dam authorities. One problem when applying cohesion in calculations, however, is to determine the compressive zone of the dam. Assuming a linearly distributed normal stress seemed to overestimate the compressive area compared to the results from the finite element analysis, indicating that the latter might be the best tool for this purpose.

Sammendrag

Skjærstyrken til et glideplan mellom betong og fjell under en dam består av to deler: friksjon fra egenvekta til dammen og kohesjon fra limet i sementpastaen som binder overflatene sammen. For platedammer med lav egenvekt, så er kohesjonsstyrkene ekstra avgjørende for glidemotstanden. De norske dam-myndighetene tillater likevel ikke å bruke kohesjon i glidesikkerhetsberegninger, med mindre kohesjonsstyrken kan dokumenteres gjennom tester. Hvordan slike tester kan gjennomføres blir derimot ikke nevnt.

Hovedmålet med denne oppgaven er derfor å utvikle og foreslå en testmetode for å estimere kohesjonsstyrken til norske platedammer. Den foreslåtte metoden benytter fjellprøver fra damstedet til å ta inn den opptredende ruheten og styrken i fjellet. Videre blir prøvene bearbeidet og betong tilsvarende dammens betong blir støp mellom de naturlige overflatene av fjellprøvene. En serie med skjærtester måler så skjærstyrken til kontaktflatene mellom betong og fjell. Kohesjonsverdien blir til slutt ekstrapolert ut fra τ-σ-kurven. Preliminær testing avdekket viktigheten av å bearbeide prøvene godt på forhånd, men etterlot forfatteren optimistisk med tanke på metodens fremtid.

For å undersøke effekten av å inkludere ruhet i beregninger ble glidesikkerheten til en av Statkraft platedammer, dam Kalhovd, analysert med en kombinasjon av elementmetodeanalyse og forenklede håndberegninger. Resultatene viste at med å anta fornuftige kohesjonsverdier, så klarte dammen å komme innenfor kravene fra de norske dam-myndighetene. Et problem ved å benytte kohesjon i beregninger er derimot å bestemme trykksonen på dammen. Å anta lineært fordelte normalspenninger virket å overestimere trykksonen sammenlignet med resultatene fra elementmetodeanalysen, noe som antyder at elementmetoden kanskje er det mest egnede verktøyet for dette formålet.

Preface

This thesis have been written as the final assessment of my 5-year Master's degree at the Department of Hydraulic and Environmental Engineering at the Norwegian University of Science and Technology.

Although working with this thesis have been challenging and frustrating from time to time, in the end it has been five really interesting and rewarding months.

I would like to thank my supervisor Leif Lia, who through many inspiring lectures motivated me to specialize and work with hydropower and dam safety. Furthermore, I would like to extend my gratitude to Statkraft and my co-supervisor Harald Andreas Simonsen, who helped to give my work a touch of real world relevancy.

Additionally, I would like to thank Rolv Guddal at Sira-Kvina, Odd Kristian Nerdahl and Steinar Seehuus at NTNUs structural lab, Geir Tesaker at NTNUs hydraulic lab and Gabriel Sas at Norut, for their contributions as well.

Trondheim, June 10th 2016

André Nymo

Table of contents

List of figures

List of tables

1. Introduction

1.1 Background

During the early 1900th, the Norwegian engineer Nils Ambursen invented the flat-slab buttress dam, also called the Ambursen dam. The dam consists of two structural elements: a flat slab taking the water pressure and buttresses that support the slab and transfer the load down into the foundation. The design aims to minimize the concrete usage, thus making it a popular choice for Norwegian dam owners with scarce resources. The drawback with this dam type, however, is that with a low self-weight the available friction resistance against sliding usually is quite small. Consequently, many older flat-slab buttress dams fail to meet the modern sliding stability criterion given by the Norwegian dam authorities. However, the criterion used neglects the cohesive strength of the concrete-rock interface coming from the glue in the cement paste, unless the strength be documented.

In order to avoid costly rehabilitation projects for dams that, in reality, are stable against sliding, a method for documenting the cohesion is wanted.

1.2 Objectives

The main scope of this thesis have been to test and come up with a reliable method to estimate the cohesion between the concrete and the rock for flat-slab buttress dams.

A secondary objective have been to estimate the available shear strength of Kalhovd dam, one of Statkrafts flat-slab buttress dams located Telemark, to see the effect of including cohesion in the calculations.

1.3 Method

The development of the testing methodology for documenting cohesion have consisted of the following main steps:

- A preliminary testing methodology was developed through a combination of literature studies and discussion with lab personnel at the structural lab at NTNU and the supervisors.
- The preliminary methodology was tested at the structural lab at NTNU.
- The results of the tests were analysed and an improved methodology have been proposed based on the experiences from the preliminary testing.

Furthermore, to assess the sliding stability of Kalhovd dam the following steps have been carried out:

- Field trip to the dam to assess the condition and geometry of the dam, the bedrock geology and pick a buttress for analysis.
- A FE-analysis of selected the buttress been carried to assess the stress distribution.
- Based the found stress distribution, the factor of safety was calculated using two different shear models.

1.4 Extent and limitations

In general, sliding of concrete dams is a three dimensional problem. However, to understand the 3D-effects, you first have to understand the 2D-effects. Thus, only sliding in a two dimensional space is considered. Additionally, the focus of this thesis have been on the sliding capacity of the concrete-rock interface. Consequently, potential sliding planes in the concrete or rock are not taken into account.

1.5 Structure

This thesis consists of five chapters in total. The first chapter contains a brief introduction of the objective, method, limitations and structure of the thesis.

The second chapter is literature review of different analysis methods for assessing sliding stability and the shear strength of unbonded and bonded concrete-rock interfaces.

In the third chapter, a stability analysis of Kalhovd dam have been carried out with both the finite element software Abaqus and hand-calculations.

The fourth chapter presents the development of the testing methodology for documenting cohesion. This chapter contains both the preliminary testing, the results and the proposed testing procedure.

At the last chapter, a conclusion of the master's work is presented, in addition to a proposal for further work.

2. Literature Review

2.1 Introduction

For concrete dams founded on bedrock, the shear capacity is a function of various parameters. From the authors specialization project (Nymo 2015) the shear resistance was found to b, at least influenced, by surface roughness, the applied normal stress and the degree of bonding and cohesion between the rock and concrete. Furthermore, the weakest sliding plane for a concrete dam is not necessarily in the concrete-rock interface. It might as well be a weakness plane in the concrete, typically a construction joint, or in weakness plane in the rock foundation beneath the dam. However, as mentioned in chapter 1.4, this thesis will focus mainly on the shear strength and failure mechanisms of the concrete-rock interface. To give both the author and the reader an understanding of the different methods of assessing sliding stability and the shear strength of concrete-rock joints, a thorough literature review is presented.

2.2 Analysis Methods

During the last 100 years of dam building, there has been several different approaches to analyse the sliding stability of concrete dams. The three most used methods is the sliding resistance method, the shear friction method and the limit equilibrium method.

2.2.1 The Sliding Resistance Method

In 1933, Henny published an important paper on the topic of sliding stability of dams (cited in Nicholson 1983). According to Henny, before the 1930s, the following safety criterion was commonly used for dam safety analysis:

$$FS = \frac{P}{W - u} \tag{2.1}$$

where *FS* is the factor of safety, *P* is the driving horizontal forces, *W* is the self-weight of the dam above the assumed sliding plane and *u* is the uplift force of the dam. This method is often

referred to in literature as the *sliding resistance method*. How the factor of safety was selected is not clearly given in literature (Nicholson 1983).

2.2.2 The Shear Friction Method

In his paper from 1933, Henny also presented a new method to calculate the safety against sliding. The method is called the *shear friction method* and it was derivated by combining the Coulomb failure criterion and the general expression for the sliding safety of a dam:

$$FS = \frac{S}{P} \tag{2.2}$$

where *S* is the total shear capacity of the plane and *P* is the total driving horizontal forces.

Expressing S with the Coulomb equation gives

$$S = s_1 + k(W - u) \tag{2.3}$$

where s1 is the total shear capacity without loading, k is a factor of increase in shear strength, W is the total weight of the dam and u is the uplift forces on the dam,

By combining equation (2.2) and (2.3) Henny developed an expression for the safety factor against sliding for a horizontal dam:

$$FS = \frac{s_1 + k(W - u)}{P} \tag{2.4}$$

In modern literature, equation (2.4) is usually given on the following form:

$$FS = \frac{c \cdot A + \sum V' \cdot \tan \phi}{\sum H} \tag{2.5}$$

with the following parameters:

FS = the factor of safety

c = cohesion

A = contact area between dam and foundation

$\sum V'$ = the sum of effective vertical forces on the dam

$\sum H$ = the sum of horizontal forces on the dam

ø = the friction angle between the dam and the foundation

The U.S. Army Corps of Engineers extended the shear friction model to include inclined sliding planes and embedment toe resistance (Nicholson 1983). The new factor of safety hence became:

$$FS = \frac{R + P_p}{\sum H} \tag{2.6}$$

where *R* is the maximum horizontal force the potential failure plane below the dam can resist and P_P is the maximum passive resistance of a rock wedge located at the dam toe.

For an upslope sliding problem *R* is:

$$R = \sum V' \cdot \tan(ø + \alpha_s) + \frac{c_s \cdot A_s}{\cos \alpha_s \cdot (1 - tan\, ø \cdot \tan \alpha_s)} \tag{2.7}$$

where α_s is the angle between the inclined sliding plane of the dam and the horizontal plane.

For a downslope sliding problem *R* becomes:

$$R = \sum V' \cdot \tan(ø - \alpha_s) + \frac{c_s \cdot A_s}{\cos \alpha_s \cdot (1 + tan\, ø \cdot \tan \alpha_s)} \tag{2.8}$$

The equation for the passive wedge resistance P_P is according to Nicholson:

$$P_p = W' \cdot \tan(ø + \alpha_P) + \frac{c_P \cdot A_P}{\cos \alpha_P \cdot (1 - tan\, ø \cdot \tan \alpha_P)} \tag{2.9}$$

where *W'* is the effective weight of the passive rock wedge at the dam toe and α_P is the angle of the inclined sliding plane of the passive wedge and the horizontal plane.

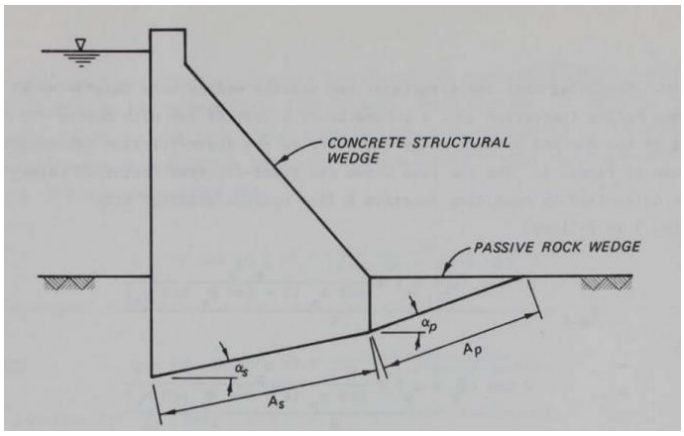

Figure 2.1: Illustration of a concrete dam with a passive rock wedge (From Nicholson 1983).

2.2.3 Limit Equlibrium Method

The limit equilibrium method uses geotechnical properties based on the shearing resistance of soil and rock to calculate the safety factor (Nicholson 1983):

$$FS = \frac{\tau_F}{\tau} \tag{2.10}$$

where FS is the factor of safety, τ_F is the available shear strength, and τ is the shear strength required for equilibrium. Thus, the dam is stable against sliding when the resultant of the shear stresses necessary for equilibrium is less than the maximum mobilizable shear strength.

Nicholson (1983) listed seven assumptions required to be fulfilled for the method to be valid:

1. The factor of safety is defined by equation (2.10)
2. Impending failure occurs according to the requirements imposed by elastic-plastic failure theory
3. The maximum shear strength that can be mobilized is adequately defined by the Mohr-Coulomb failure criteria
4. Failure modes can be represented by two-dimensional, kinematically possible planes
5. The factor of safety computed from the stability equations is the average factor of safety for the total potential failure surface.
6. To derive easy, simple-to-use equations, the vertical stresses/forces acting between wedges or slices are assumed to be negligible
7. The structural wedge must be defined by only one wedge

This method can be further expanded to assess multiple wedges as shown in the figure below:

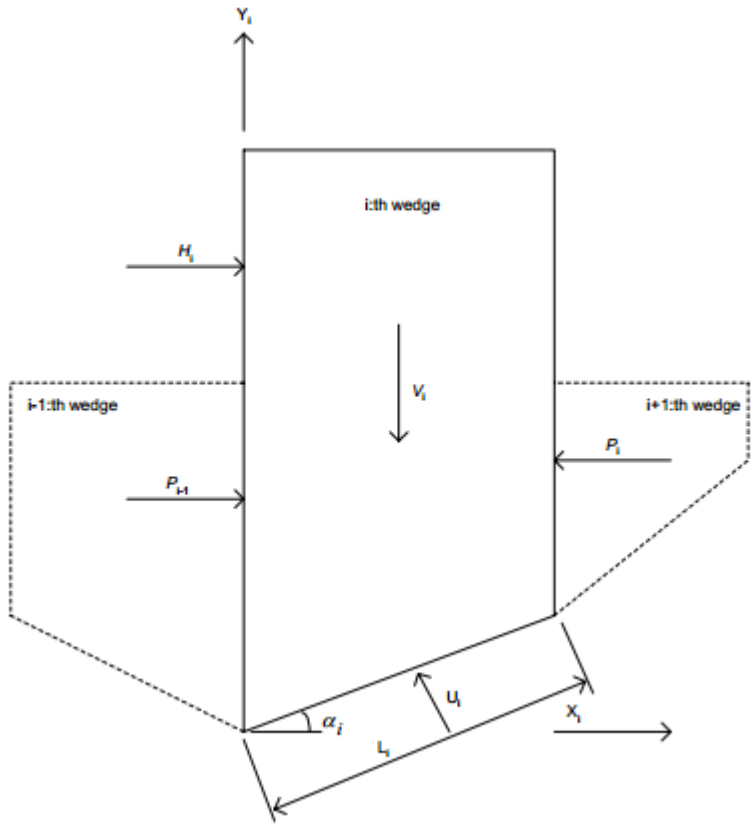

Figure 2.2: Geometry, forces, and coordinate system for an ith wedge in a hypothetical wedge system (from Johansson 2009) based on Nicholson (1983).

The force difference between wedge *i* and *i-e* for the figure above can be expressed by the following formula (Nicholson (1983)):

$$(P_{i-1} - P_i) = \frac{(V_i \cdot \cos\alpha_i - U_i + H_i \cdot \sin\alpha_i) \cdot \frac{\tan\phi_i}{FS_i}}{(\cos\alpha_i - \sin\alpha_i \cdot \frac{\tan\phi_i}{FS_i})} - \frac{H_i \cdot \cos\alpha_i + V_i \cdot \sin\alpha_i + \frac{c_i}{FS_i} \cdot L_i}{(\cos\alpha_i - \sin\alpha_i \cdot \frac{\tan\phi_i}{FS_i})} \quad (2.11)$$

P = horizontal force acting on the vertical face of a wedge

V_i = sum of the vertical forces acting on wedge *i*

U_i = sum of the uplift forces acting on wedge *i*

H_i = sum of external horizontal forces acting on wedge *i*

α_i = angle between horizontal plane and sliding plane for wedge *i*. Positive for upwards sliding, negative for downward sliding.

FS = factor of safety

L_i = length of the wedge along the sliding plane

c = cohesion

ø = friction angle for the rock

By demanding that the factor of safety is equal for all parts of a system of *n* wedges, the result is *n* equations with *n+1* unknowns satisfying

$$FS_i = FS_1 = FS_2 = \ldots = FS_n \tag{2.12}$$

where FS_i = the safety factor for wedge i.

This system can then be solved by applying an equation demanding horizontal equilibrium between the wedges such that

$$P_{i-1} - P_i = P_B \tag{2.13}$$

where P_B is the boundary forces between the wedges. For most cases the boundary forces P_B are zero, thus the problem can be solved by a using the conditional equation:

$$\sum_{i=1}^{n} (P_{i-1} - P_i) = 0 \tag{2.14}$$

The factor of safety can then be calculated by guessing a solution for FS in equation (2.8) until equation (2.11) is fulfilled.

Nicholson also suggested an alternative equation making it possible to calculate the factor of safety directly:

$$FS = \frac{\sum_{i=1}^{n} \frac{c_i \cdot A_i \cdot \cos\alpha_i + (V_i - U_i \cdot \cos\alpha_i) \cdot \tan\phi_i}{n_{\alpha i}}}{\sum_{i=1}^{n} (H_i - V_i \cdot \tan\alpha_i)} \tag{2.15}$$

Where A_i is the area of the sliding plane for wedge *i*, $n_{\alpha i}$ is as defined by equation (2.13) and the other variables are as defined for equation (2.8).

$$n_\alpha = \frac{1 - \frac{\tan \phi_i \cdot \tan \alpha_i}{SF}}{1 + \tan^2 \alpha_i} \tag{2.16}$$

2.3 Shear Strength and Failure criterions

Shear strength of concrete-rock foundations is basically a frictional problem. Amontons' friction model from late 1700th century states that the frictional force F_f on a moving object is proportional to the normal force F_n with the proportionality constant, often referred to as coefficient of friction μ:

$$F_f = \mu \cdot F_n \tag{2.17}$$

Amontons' model generalized for stresses gives the following expression:

$$\tau = \mu \cdot \sigma_n \tag{2.18}$$

where τ is the shear stress and σ_n is the normal stress.

In the 18th century, Coulomb century investigated the shear capacity of soil materials and came up with the Coulomb strength theory (Golder 1948). According to Coulombs strength theory the shear strength of two materials can be divided in two: a cohesion part, representing the internal molecular attraction between the materials (shear strength with no applied normal stress), and a friction part, representing the lateral motion resistance between two surfaces. Coulomb agreed with Amontons regarding the proportionality of the friction and the normal force (Golder 1948). Furthermore, he stated that the total cohesion is proportional to the area of the surface of rupture.

At the end of the 19th century, Mohr developed a generalized form of Coulombs strength theory using Mohr circles (S.A. Miedema. 2014). Consequently, the combined strength theory is commonly referred to as the Mohr-Coulomb strength theory. In modern literature the Mohr-Coulomb failure criterion is usually given on the form

$$\tau = c + \sigma_n \cdot \tan \phi \tag{2.19}$$

where τ is the shear strength, c is the cohesion, σ is the normal stress and ø is the angle of internal friction.

The Mohr-Coulomb failure criterion have since been adopted to describe the shear strength of brittle materials as concrete and rock. The failure criterion assumes a linear relationship between the normal stress and the shear capacity. However, shear tests of concrete-rock joints exhibit a curvilinear τ-σ relationship, both for bonded and unbonded joints (Donnelly et al 1996). Furthermore, cohesive bonds giving the cohesive additive strength are only present for bonded concrete-rock joints. Once the structure start to deform significantly, these bonds are broken, and only the friction resistance is left to withstand the deformation. Hence, the failure behaviour and peak shear capacity of bonded and unbonded joints are very different, as illustrated by figure 2.3. It is therefore essential to distinguish between bonded and unbonded surfaces when assessing the shear capacity of concrete dams.

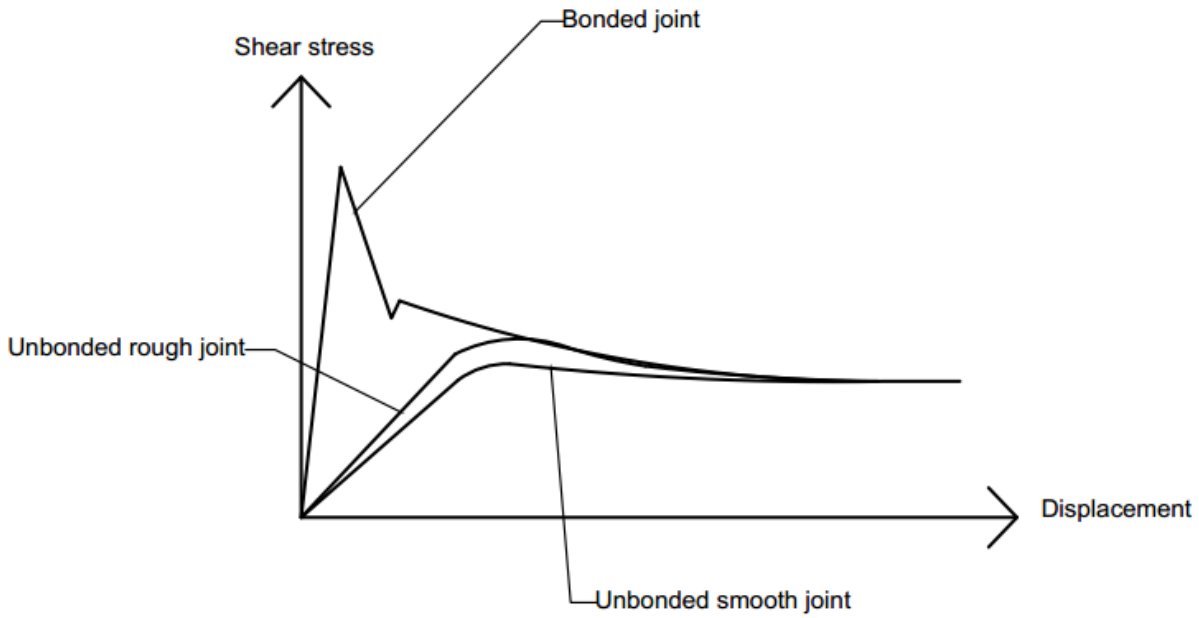

Figure 2.3: Typical stress-displacement curves for bonded, unbonded smooth and unbonded rough joints

2.3.1 Shear Strength for Unbonded Concrete-Rock Joints

Most research on unbonded concrete-rock joints proceed on earlier work done on rough rock-rock joints due to the similar nature of the materials. Originally, the peak strength of rough (non-planar) rock joints was assumed to increase linearly with increasing normal load as described by the Mohr-Coulomb criterion. However, studies done during in the mid-twentieth century suggested a curved strength curve for rough discontinues due to an added dilatational resistance for low normal stresses (Jaeger 1959; Lane and Heck 1964; Patton 1966; among

others). Some of the most important models for estimating the shear strength of rough rock joints are presented in this chapter.

Patton (1966) performed over 200 direct shear test of artificially made laboratory specimens with varying geometry. The result was a strength criterion that considers the roughness through an average asperity angle *i* along the interface:

$$\tau = \sigma_n' \cdot \tan(\phi_b + i) \tag{2.20}$$

τ is the total shear strength

σ_n is effective the normal stress

ϕ_b is the basic friction angle, defined as the friction angle of a smooth flat surface.

i is the inclination angle of the failure interface

This criterion is, however, only valid for small normal loads. For rock joints subjected to higher normal stress, the internal shear capacity of the rock become the governing factor for the overall sliding resistance. The reason for this is a change in failure mode from sliding over the asperities to shearing through them. Thus, the strength criterion becomes

$$\tau = c_x + \sigma_n' \cdot \tan(\phi_r) \tag{2.21}$$

where τ is the total shear strength, c_x is the internal cohesion in the rock asperities, σ_n' is the effective normal stress and ϕ_r is the residual or weathered friction angle. The change in failure modes is illustrated in figure 3.1 by the change of slope in the failure envelope:

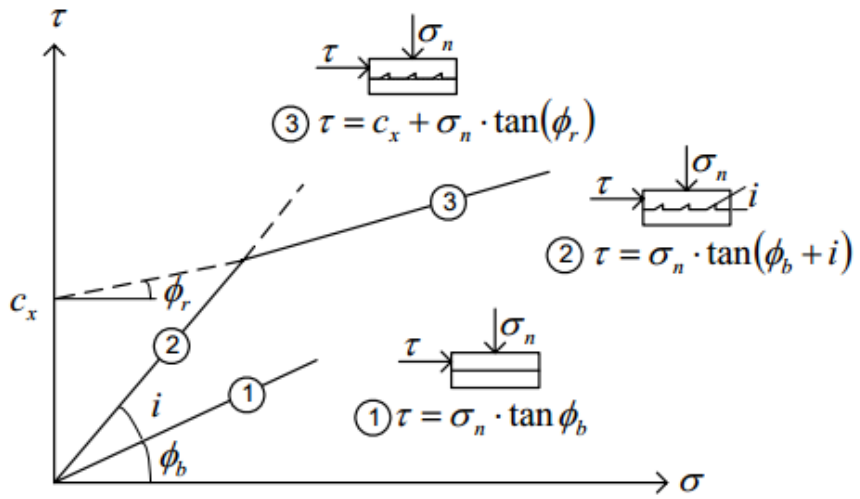

Figure 2.4: Bilinear failure curve proposed by Patton (from Johansson 2009)

Patton (1966) emphasized, however, that for a real rock sample there is not one simple change of failure modes, but rather a change "*in the "intensities" of different modes of failure occurring simultaneously*" due to variances in size, inclination, internal strengths and friction coefficients in irregular asperities along the surface.

In order to account the irregularity of the surface roughness Ladanyi and Archambault (1969) developed a model with basis in energy considerations, instead of the more common statistical methodology.

By looking at the shearing along an interface, and assuming no shearing through the asperities, they described the total shearing force S as a sum of three components:

$$S = S_1 + S_2 + S_3 \tag{2.22}$$

S_1 = component due to external work in dilating against the external force N
S_2 = component due to additional internal work in friction caused by dilatancy
S_3 = component due to work done in internal friction if sample did not change volume in shear

S_1 can be defined from rearranging the work equation:

$$S_1 = N \cdot \frac{dy}{dx} = N \cdot \acute{\upsilon} \tag{2.23}$$

where $\acute{\upsilon}$ is the dilation rate at failure defined as the ratio between the increments of the normal displacement *dy* and the shear displacement *dx* at failure and N is external the normal force on the rock. Figure 2.5 shows an graphical illustration of the dilation rate. S_1 is the same as $N \cdot \tan i$ for a regular tooth formed asperity and it becomes zero for smooth plane sliding interface.

A rough shearing interface will create an additional shearing force

$$S_2 = S \cdot \acute{\upsilon} \cdot \phi_f \tag{2.24}$$

where ϕ_f defined as an statistical average value of the friction angle when sliding occurs along irregularities of different orientations and S is the external shearing force. According to Ladanyi and Archambault (1969) ϕ_f will not vary much from the friction angle of the rock along the shearing interface ϕ_μ for initially well interlocked rock interfaces that becomes significantly dilatant at failure.

S_3 is the friction component for a flat rough surface exposed to the normal force N

$$S_3 = N \cdot \tan \phi_\mu \tag{2.25}$$

Furthermore, they defined a fourth shear force component S_4 describing shearing through the asperities as

$$S_4 = A \cdot s_0 + N \cdot \tan \phi_0 \tag{2.26}$$

where A is the projected shear area, where s_0 is the internal cohesion strength of the intact rock material and ϕ_0 is the friction angle of the intact rock material.

As both the failure modes, sliding across and shearing through the asperities, can happen simultaneously, it was necessary to define a shear area ratio

$$a_s = A_s/A \tag{2.27}$$

where A_s is the portion of area where asperities are sheared off and A is the total projected area.

Thus, the total shearing force S describing both failure modes can be rewritten as

$$S = (S_1 + S_2 + S_3)(1 - a_s) + S_4 \cdot a_s \tag{2.28}$$

By inserting eq. (2.23), (2.24), (2.25) and (2.26) into eq. (2.28) and dividing with the area A, an expression for the shear stress τ is found:

$$\tau = \frac{S}{A} = \frac{\sigma (1 - a_s)\left(\dot{\upsilon} + \tan \phi_\mu\right) + a_s (\sigma \cdot \tan \phi_0 + s_0)}{1 - (1 - a_s)\, \dot{\upsilon} \cdot \tan \phi_0} \tag{2.29}$$

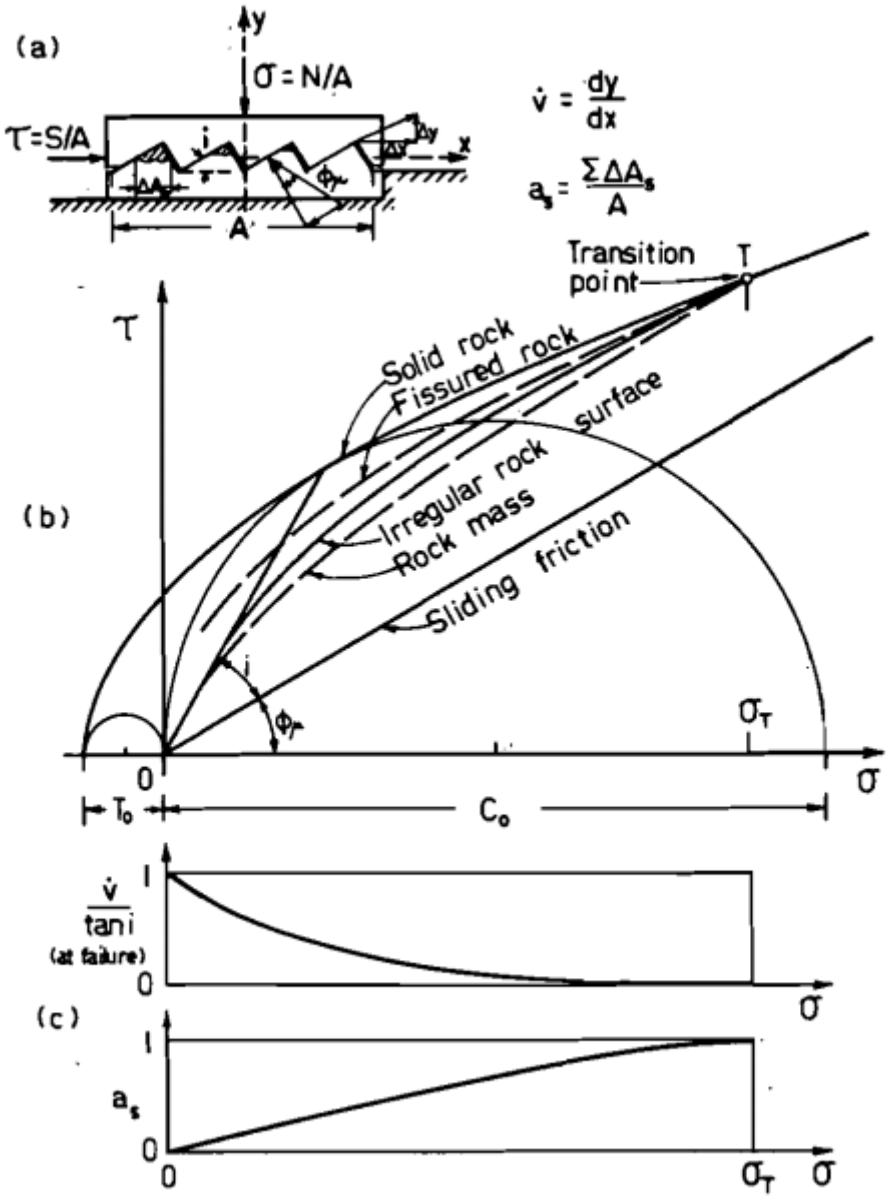

Figure 2.5: A graphic illustration of the basic assumptions and anticipated results for the proposed failure model. (a) Definition of the dilation rate and the shear area rate. (b) Anticipated failure envelopes for irregular rock surfaces and rock mass, respectively. (c) Anticipated variation of the dilation rate and shear area rate with normal pressure (from Ladanyi and Archambault 1969).

This expression is, however, according to Ladanyi and Archambault (1969) only valid under the assumption of tightly closed cracks and complete interlocking. These assumptions are not necessarily valid for natural rock profiles exposed to, for instance, creep, variable water levels, weathering or stress relief. To account for variances in the interlocking they introduced a degree of interlocking η given by

$$\eta = 1 - \Delta x/\Delta L \tag{2.30}$$

where Δx is length of the shear displacement and ΔL is the projected length of the asperities in the shear direction. See figure 2.6 for a graphical illustration of the degree of interlocking.

Thus, the true projected area A_t can be described by $A \cdot \eta$, and eq. (2.29) becomes

$$\tau = \frac{S}{A} = \frac{\sigma\,(1 - a_s)\left(\acute{\upsilon} + \tan \phi_\mu\right) + a_s\,(\sigma \cdot \tan \phi_0 + s_0 \cdot \eta)}{1 - (1 - a_s)\,\acute{\upsilon} \cdot \tan \phi_0} \tag{2.31}$$

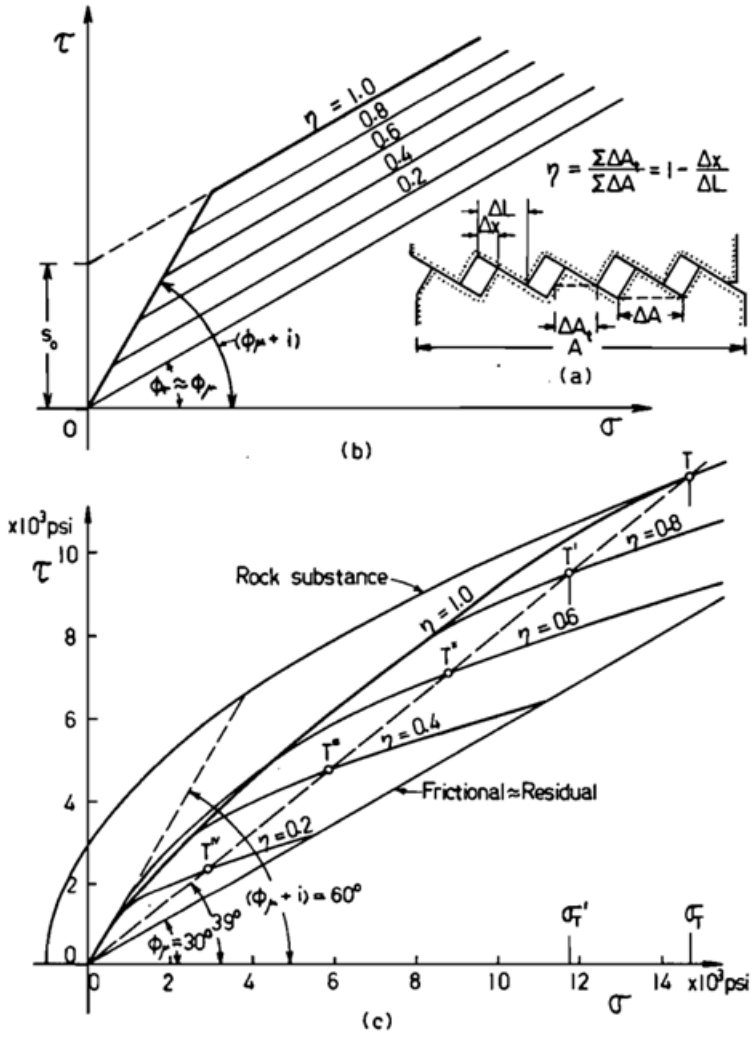

Figure 2.6: Effects of reducing the degree of interlock. (a) Definition of the degree of interlocking. (b) Results according to the bilinear model. (c) Results according to the proposed model (from Ladanyi and Archambault 1969).

To estimate a_s and ύ, Ladanyi and Archambault (1969) suggested using the following empirical approximations probable variation of the parameters within the interval $0 < \sigma < \sigma_T$ for the normal stress:

$$a_s \approx 1 - (1 - \frac{\sigma_T}{\eta \cdot \sigma_T})^{k_1} \tag{2.32}$$

$$\acute{\upsilon} \approx \left(1 - \frac{\sigma_T}{\eta \cdot \sigma_T}\right)^{k_2} \cdot \tan i \tag{2.33}$$

Using the available experimental data the exponents where approximated to $k_1 \approx 1{,}5$ and $k_2 \approx 4$. Comparing with the available empirical data, the model managed to describe the relative contributions from most of the important parameters for the total shear strength of irregular rock joints (Ladanyi and Archambault 1969). The authors underlined, however, that more experimental data was necessary to further validate the model.

Barton (1973) and Barton and Choubey (1977) developed a non-linear empirical failure criterion, often called the JRC-JCS joint model. The criterion was established using data from numerous direct shear tests on rock joints.

By plotting the peak friction angle $\phi = \tan^{-1}(\frac{\tau}{\sigma_n})$ against the peak dilation angle d_n, Barton (1973) developed the following relationship

$$\tau = \sigma_n \cdot \tan(2\, d_n + 30°) \tag{2.34}$$

where τ is the peak shear stress, σ_n is the normal stress and d_n is the peak dilation angle, which is the instantaneous inclination d*v*/d*h* of the shearing path at peak strength, relative to the mean plane.

In addition, he discovered that the peak dilation angle was proportional to the logarithm of the ratio between the unconfined compression strength and the normal stress:

$$d_n = 10 \log(\frac{\sigma_c}{\sigma_n}) \tag{2.35}$$

By inserting equation (2.35) into (2.34) the earliest expression of the failure criteria was created:

$$\tau = \sigma_n \cdot \tan(20 \log(\frac{\sigma_c}{\sigma_n}) + 30°) \quad (2.36)$$

By replacing 30° with the basic friction angle ϕ_b the expression was generalized to

$$\tau = \sigma_n \cdot \tan(20 \log(\frac{\sigma_c}{\sigma_n}) + \phi_b) \quad (2.37)$$

Barton (1973) further argued that weathering of the joint would reduce the compressive strength, thus using the unconfined compression strength σ_c would only be valid for completely unweathered rock joints. Consequently, he introduced the effective joint wall compressive strength JCS, which is the actual compressive strength measured on the joint itself, to replace σ_c in weathered joints. Barton and Choubey summarized the weathering process of rocks in the following basic steps:

1) Formation of joint in intact rock; No weathering means JCS value are the same as the unconfined compression strength σ_c.
2) Slow reduction of joint wall strength if joints are water-conducting; JCS become less than σ_c.
3) Common intermediate stage; weathered, water-conducting joints, impermeable rock blocks between, JCS is some fraction of σ_c.
4) Penetration of joint weathering effect into rock blocks; progressive reduction of σ_c from the walls of the blocks inwards, JCS continues to reduce slowly.
5) Advanced stage of weathering; more uniformly reduced σ_c finally drops to the same level as JCS; rock mass is permeable throughout.

According to Barton and Choubey (1977) the JCS value can be estimated by using, for instance, the Schmidt hammer rebound test.

Furthermore, it was necessary to take into account joints with lower degrees of roughness than those considered above. This is rock joints, which according to Barton (1973), lie somewhere in between the brittle-fracture tension joints and the smooth residual shear interfaces. Therefore, the joint roughness coefficient JRC was presented as a measure on the roughness along the joint. The JRC varies from 0 (smooth) to 20 (rough) depending on the

roughness profile. The value can be estimated through visual inspection and comparison with the predefined roughness profiles given in figure 2.7. However, as this method is highly subjective, Barton and Choubey (1977) argued that the most satisfactory procedure is tilt tests on rock samples from site, and back calculation of the actual JRC-value.

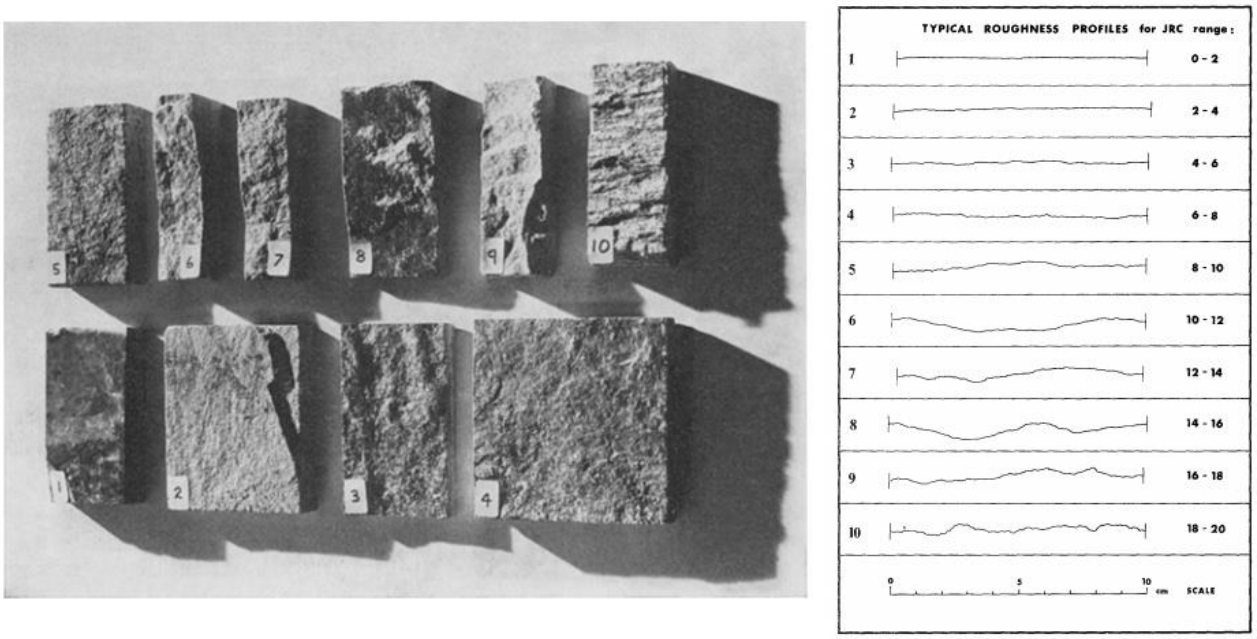

Figure 2.7: Typical roughness profiles (from Barton and Choubey 1977)

Hence, Barton (1973) presented the following equation to estimate the peak shear strength of rough rock joints, also taking into account the variances in surface roughness and weathered compressive strength:

$$\tau = \sigma_n \cdot \tan[JRC \cdot \log_{10}(\frac{JCS}{\sigma_n}) + \emptyset_b] \tag{2.38}$$

where

JRC is the joint roughness coefficient, varying from 0 (smooth) to 20 (rough)

JCS is the effective joint wall compressive strength

σ_n is the normal stress.

$\emptyset_b$ is the basic friction angle

Barton and Choubey (1977) later argued that the basic friction angle $\emptyset_b$ from equation (2.38) should be replaced with the residual friction angle $\emptyset_r$, which represents the minimum shear capacity. The reason being that most of the values of $\emptyset_b$ is obtained from unweathered rock specimen which are saw-cut, and in many cases also sandblasted. Furthermore, the test results

from 136 joints showed a significant reduction in the friction angle due to weathering. The result is the following updated expression for the general peak shear strength:

$$\tau = \sigma_n \cdot \tan[JRC \cdot \log_{10}(\frac{JCS}{\sigma_n}) + \phi_r] \tag{2.39}$$

To estimate the residual friction angle the authors (Barton and Choubey 1977) suggested using Schimdt rebound tests combined with the empirical relationship between ϕ_r and the basic friction angle ϕ_b:

$$\phi_r = (\phi_b - 20°) + 20 \cdot \left(\frac{r}{R}\right) \tag{2.40}$$

where R is the Schmidt rebound on dry unweathered sawn surfaces and r is the Schmidt rebound on wet joint surfaces.

They also mentioned that for smooth plane joints or joints that present signs of early movement, the sole shear strength would have be based on ϕ_r for design purposes, as the joints cannot be expected to have any asperity or roughness contribution to the shear capacity. On the other side, if the joints are non-planar (rough), not presheared and some measures (as i.e bolts) are taken to stop further deformations, the peak dilation angle will give an estimate off the additional shear capacity beyond ϕ_r. Hence, the total friction angle should be at least equal to the sum of the residual friction angle and the peak dilation angle. In other words:

$$\phi_r + d_n \leq \tan^{-1}(\frac{\tau}{\sigma_n}) \tag{2.41}$$

According to Barton and Choubey the total shear resistance is likely higher than just the sum of ϕ_r and d_n since the additional capacity from crushing of the asperities is neglected.

Barton and Bandis (1983) argued that the shear strength and shear stiffness is reduced with increasing specimen size. The reason is a reduction in effective joint roughness and asperity strength. Using the results from widespread testing of joints, joint replicas and literature reviews, they proposed the following empirical equations for scale corrections:

$$JRC_n \approx JRC_o \left[\frac{L_n}{L_o}\right]^{-0.02JRC_o} \tag{2.42}$$

$$JCS_n \approx JCS_o \left[\frac{L_n}{L_o}\right]^{-0.03JRC_o} \tag{2.43}$$

where L is the length of the sample or rock joint and the subscripts (o) and (n) refer to lab scale (100mm) and in situ size, respectively.

Grasselli (2001) developed a strength criteria by comparing test results from direct shear tests with measurements of the surface roughness using a three-dimensional scanning device called ATS (Advanced Topometric System). The device measured the surface as point clouds and a triangulation algorithm reconstructed the surface as a finite number of triangles. He proposed that only the triangles facing the shear direction influenced the shear capacity. This was also in line with the test results, where inspection afterwards showed that only the steepest zones facing the shear direction exhibited visible damage. Grasselli introduced a parameter he called the apparent dip angle θ^*, which describes the contribution of the projected inclination of each triangle. A geometrical explanation of θ^* can be seen in figure 2.8.

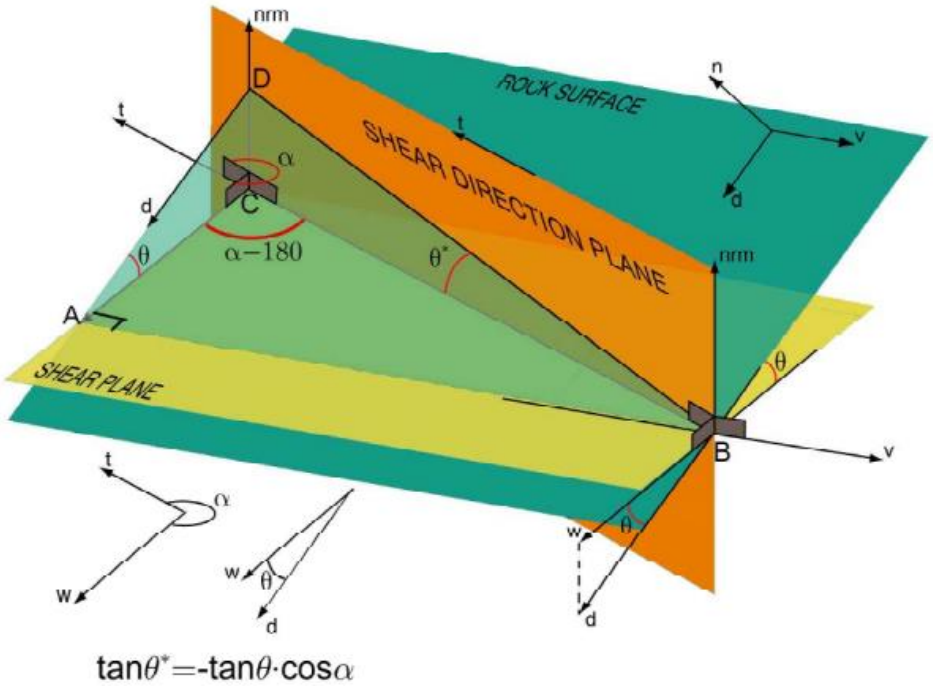

Figure 2.8: Geometrical identification of the apparent dip angles, in function of the shear direction (From Grasselli 2001)

Grasselli named the sum of the area of all the triangles the potential contact area A_c. Using regression, he proposed the following expression for estimatingA_c:

$$A_c = A_o \cdot \left[\frac{\theta^*_{max} - \theta^*}{\theta^*_{max}}\right]^C \tag{2.44}$$

where A_o is the maximum possible contact area against the sliding direction, θ^*_{max} is the maximum dip angle, θ^* is the apparent dip angle and C is a roughness parameter describing the concavity of the $A_c - \theta^*$ curve. According to Grasselli (2001), the laboratory tests show θ^*_{max} varying from 20° to 90° for natural rock surfaces.

Studying the test results, Grasselli argued that the tensile strength σ_t of the rock is more vital to the sliding capacity than the compressive strength, due to the nature of the failure mechanism. By using the results from his direct shear tests, he suggest the following equation for the peak shear strength of rock joints:

$$\tau_p = \sigma_n \cdot \tan(\phi'_r) \cdot (1 + g) \tag{2.45}$$

where σ_n is the average normal stress and ϕ'_r is the residual friction angle. g is an expression describing the surface morphology:

$$g = e^{\frac{-\theta^*_{max}}{9 \cdot A_o \cdot C} \cdot \frac{\sigma_n}{\sigma_t}} \tag{2.46}$$

with parameters described earlier.

To estimate the residual friction angle ϕ'_r ,Grasselli (2001) proposed an empirical formula including the basic friction angle ϕ_b:

$$\phi'_r = \phi_b + \left(C \cdot {A_o}^{1.5} \cdot \theta^*_{max} \cdot \left(1 - A_o^{1/C}\right)\right)^{\cos\alpha} \tag{2.47}$$

where α is the angle between the schistosity plane and the normal plane to the joint. If no schistosity plane exist α is set to zero. The other parameters are the same as described earlier.

Johansson (2009) and Johansson and Stille (2014) came up with a conceptual model to describe the dilation angle or the asperity angle *i* for full sized joints. The model is based upon sliding over the asperities as the dominating and governing failure mode. Thus, the peak shear strength can be described by:

$$\tau = \sigma'_n \cdot \tan(\emptyset_b + i_n) \tag{2.48}$$

where σ'_n is the effective normal stress, $\emptyset_b$ is the basic friction angle and i_n is the dilation angle for a full sized joint.

Johansson (2009) explained the shearing mechanism as followed

"When shearing is initiated for a perfectly mated, unfilled and rough joint, subjected to a constant normal load, the asperities will first be deformed elastically. At the same time, the load at the initial contact points starts to increase and quickly reaches the yield strength of the material. At this point, the smallest asperities facing the shear direction will be crushed since the potential contact area for these asperities are too small to carry the total load."

Furthermore, he stated that this process would continue successively until a critical number of the asperities are reached, and the potential contact area becomes the same as the true contact area. At this point, the measured dip angle θ^* of the contacting asperities can be set equal to the dilation angle of the joint surface at grain size *i* (Johansson and Stille 2014).

From adhesion theory of friction, the true area of contact $A_{c,r}$ can be expressed as the quotient between the effective normal stress and the yielding stress of the joint surface, σ_{ci}:

$$A_{c,r} = \frac{\sigma'_n}{\sigma_{ci}} \tag{2.49}$$

Furthermore, the potential contact area ratio $A_{c,p}$ for a rough joint can be described empirically as proposed by Grasselli (2001):

$$A_{c,p} = A_o \cdot \left[\frac{\theta^*_{max} - \theta^*}{\theta^*_{max}}\right]^C \tag{2.50}$$

where A_o is the maximum possible contact area against the sliding direction, θ^*_{max} is the maximum dip angle measured on the sample and θ^* is the measured dip angle defined as the inclination of the asperities against the sliding direction. C is a roughness parameter.

The following relationship between the asperity height h_{asp} and base length of the asperities L_{asp} was suggested:

$$h_{asp} = a \cdot {L_{asp}}^{H} \tag{2.51}$$

where *a* is an amplitude constant and H is the Hurst exponent. Both of the factors are based on the base lengths of varying asperity orders.

Johansson (2009) argued that for a constant normal stress and true contact area, the change in the number of contact points determines how the area of the average contacting asperities change. By assuming that the contact points are quadratic shaped on the joint wall surface, Johansson therefore expressed asperity base length for a full sized joint as:

$$L_{asp,n} = L_{asp,g} \cdot \left(\frac{L_n}{L_g}\right)^{k} \tag{2.52}$$

where *L* is the length of the sample, L_{asp} is the base length of the asperity and the subscripts (g) and (n) is defined as grain size and full sized joints, respectively. *k* is an empirical constant varying between 0 (fully mated) and 1 (zero matedness), describing the degree of matedness.

By setting the potential contact area ratio $A_{c,p}$ equal to the true area of contact $A_{c,r}$, an equation for the measured dip angle θ^* can be found:

$$\theta^* = \theta^*_{max} - 10^{\frac{log\frac{\sigma_n'}{\sigma_{ci}} - logA_0}{C}} \cdot \theta^*_{max} \tag{2.53}$$

The inclination *i* can be found through geometry considerations from figure 2.9:

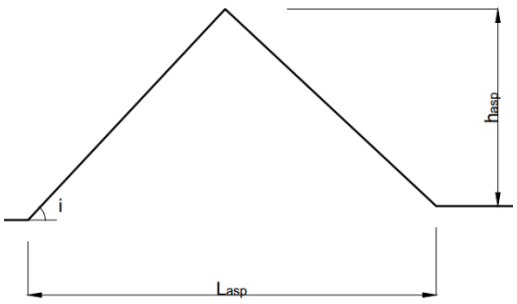

Figure 2.9: Geometry of an idealized asperity proposed by Johansson (2009).

$$i = arctan\left(\frac{h_{asp}}{0.5 \cdot L_{asp}}\right) \tag{2.54}$$

As equilibrium is reached, the measured dip angle θ^*becomes equal to the inclination of the asperities *i*, at grain size.:

$$arctan\left(\frac{h_{asp}}{0.5 \cdot L_{asp}}\right) = \theta^*_{max} - 10^{\frac{log\frac{\sigma_n'}{\sigma_{ci}} - logA_0}{C}} \cdot \theta^*_{max} \tag{2.55}$$

If equation (2.51) then is inserted into equation (2.55), an expression for the length of the asperities at grain size can be found:

$$L_{asp,g} = \left[\frac{0.5}{a}\left[\tan\left(\theta^*_{max} - 10^{\frac{log\frac{\sigma_n'}{\sigma_{ci}} - logA_0}{C}} \cdot \theta^*_{max}\right)\right]\right]^{\frac{1}{H-1}} \tag{2.56}$$

If then equation (2.51), (2.52) and (2.56) is inserted into equation (2.54) the following expression for the dilation angle for full sized joints is found:

$$i_n = arctan\left(2a\left(\left[\frac{0.5}{a}\left[\tan\left(\theta^*_{max} - 10^{\frac{log\frac{\sigma_n'}{\sigma_{ci}} - logA_0}{C}} \cdot \theta^*_{max}\right)\right]\right]^{\frac{1}{H-1}}\left(\frac{L_n}{L_g}\right)^k\right)^{H-1}\right) \tag{2.57}$$

Simplifying the equation above gives the following expression for the asperity inclination for full sized joints:

$$i_n = arctan\left[tan\left(\theta^*_{max} - 10^{\frac{log\frac{\sigma_n'}{\sigma_{ci}} - logA_0}{C}} \cdot \theta^*_{max}\right)\left(\frac{L_n}{L_g}\right)^{kH-k}\right] \tag{2.58}$$

For convenience, the definition of the parameters from equation (2.58) is repeated below:

θ^*_{max} = maximum measured dip angle on sample

k = empirical constant describing matedness varying in the range 0-1

H = the Hurst exponent

σ_n' = effective normal force on the joint

σ_{ci}= yielding strength of joint surface

C = roughness parameter

A_0 = potential contact area

L_n = length of the full sized joint

L_g = length of grain size

Using equation (2.58), Johansson (2009) managed to describe the conceptual behaviour of the dilation angle under varying scale levels:

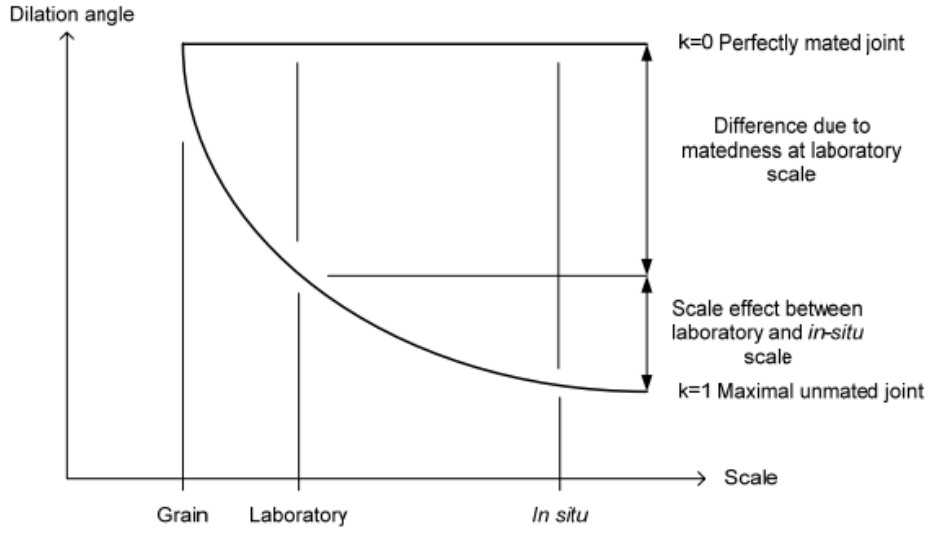

Figure 2.10: Conceptual behaviour of asperity angle with varying matedness and scale (From Johansson 2009).

According to the model propsed by Johansson (2009) and Johansson and Stille (2014) the scale effect in the dilation angle is highly influenced by the degree of matedness. For joints with low degrees of matedness, the scale effect can be quite significant, whereas for higher degrees of matedness the effect is less prominent. For a perfectly mated joint, there should be no scale effect at all, as the number of contact points increase proportionally to the area of the joint.

The conceptual model have some weaknesses, however. For instance, the yield strength of the joint surface is assumed constant and independent of the scale. In addition, it is assumed that the normal stress is monotonically increasing, thus neglecting changes in the inclination angle due to cyclic stress changes.

2.3.2 Shear Strength for Bonded Concrete-Rock Joints

In contrary to for unbonded rock joints there have not been a significant amount of studies on the sliding mechanisms governing the shear capacity for bonded rock-concrete interfaces. Most research on bonded concrete-rock foundations have traditionally been done by fitting Mohr-Coulomb failure envelopes, described by equation (2.59), to results from direct shear tests.

$$\tau = c + \sigma_n \cdot \tan \phi_i \tag{2.59}$$

c = cohesion, σ_n = normal stress, and ϕ_i = internal friction angle of contact

In 1960s, Rocha cast about 70 blocks of concrete blocks and performed in-situ tests at six different dam sites with varying rock types (cited in Ruggeri 2004). The friction angles and cohesion reported varied between 53° and 63° and 0.1 and 0.7 MPa, respectively. Weak rock masses, however, caused most of the failures to happen in parallel weakness joints in the rock foundation instead of the concrete-rock joint. Thus, the reported values somewhat underestimate the real concrete-rock strength.

Link presented a widespread tabulation of measured rock and concrete-rock strengths in 1969 (cited in Ruggeri 2004). After the results from soft marls, highly weathered rock or bedding planes were excluded ϕ_i was found to be in the range 45°-52° and c in the range 0.1 - 3.0 MPa.

The Electric Power Research Institute (EPRI) digested the results from direct shear tests on concrete-rock joints from 18 dams built between 1912 and 1965 (EPRI 1992). In total 65 cores were tested, where 35 where intact, one was unbonded and 11 sawcut. The last 18 were rock cores with concrete cast on afterwards. For the best fit lines the peak friction angle varied from 54° to 68° and for most of the rocks the cohesion varied from 1.3 to 1.9 MPa. For shale the reported cohesion was as low as 0.1 MPa.

ISMES performed shear tests on 16 large specimen to investigate the added bonding effect from interposing cement milk films in concrete-rock joints (cited in Ruggeri 2004). Two different rock types were used: a mica schist and an orto-gneiss. The results showed that the peak strength was not very affected by rock type, whereas the residual strength was.

Furthermore, using the cement milk films increased the peak shear strength, while the residual strength remained the same.

Saiang et al (2005) performed laboratory tests on shotcrete-rock joints in direct shear, tension and compression. The direct shear tests showed that for lower normal loads, typically less than 1 MPa, the shear strength of the cemented shotcrete-rock joint is primarily the bond strength. For the case of higher normal loads, the frictional resistance of the joint proved to be more dominant, whereas the cohesion became less important.

Moradian et al (2011, 2012) did direct shear tests on concrete-rock interfaces with varying bonding, normal load and displacement rate. In addition, they used acoustic emission (AE) to monitor the energy released as the tests was running. The results showed that for fully bonded joints with low normal loads, the asperities did not seem to start contributing to the sliding resistance before after the bond was broken. For fully bonded joints with higher normal loads, on the other side, the asperities and the bonding broke simultaneously.

The AE measurements showed no significant activity before reaching peak capacity and failure of the bond, thus suggesting that there was no asperity degradation before this point. Interestingly the increase in normal load from the initial 0.15 MPa to 0.65 MPa and to finally 1.25 MPa gave no noteworthy effect on the peak shear strength; it remained almost the same. The authors argued that for bonded joints with less normal load than the bond strength, the shear capacity are determined by the bond strength alone. It should be noted, however, that the normal loads were very low compared to the shear strength. Even for the highest applied normal stress (1.25 MPa), the shear capacity was higher by a factor of four (5.06 MPa). The residual strength (post failure of the bond), in contrast, increased with higher normal loads.

Furthermore, for the tests where the bonding rate was reduced, the brittle failure gradually transitioned into a softening failure due to the higher contribution from the asperities in joint failure. The reduction in bonding also led to a drop in the maximum shear strength from 4.13 MPa for 100% bonding to 1.2 MPa for 10% bonding. Additionally, the reduction in bonding also led to a gradual reduction of the residual strength after the bond is broken.

Tian et al (2014) examined the shear behaviour of bonded concrete-rock joints both experimentally and numerically. They conducted shear tests of concrete cast on smooth planar (JRC values below 2) rock samples to investigate the shear behaviour of well-bonded cohesive interfaces. The results are similar to the results of Saiaing et al (2005) and Moradian et al (2011, 2012); for low normal stress (0-2 MPa), the bond strength is dominating factor for

the peak capacity, resulting in a sudden drop in the failure curve when the bond is degraded. For higher normal loads (4-6 MPa), the failure of the bond was more gradual, and the friction played a bigger part for the overall sliding capacity. The authors estimated the internal friction angle $\emptyset_i$ of the bonded joint to be 31°, which is significantly lower than the reported value from the studies described above.

Krounis et al (2016) studied the shear capacity of partially bonded concrete rock joints. A series of 24 direct shear tests were performed with concrete-rock samples with varying bonding percentages. The purpose was to investigate the strain compatibility between the shear resistance of unbonded and bonded parts of an interface.

In the paper, the authors presented two models to estimate the shear capacity of partially bonded concrete-rock interfaces. The first one is based on work done by Lo et al (cited in Krounis et al 2016) in 1990 and 1991, and describes the peak capacity τ_p as:

$$\tau_p = A_b \cdot (c + \sigma_n' \cdot \tan \emptyset_i) + (1 - A_b) \cdot \sigma_n' \cdot \tan(\emptyset_b + i) \tag{2.60}$$

where A_b is the ratio of bonded area to total area, σ_n' is the effective normal stress, and c and $\emptyset_i$ is the cohesion and the internal friction angle of the bonded contact, respectively. $\emptyset_b$ and i is the basic friction angle and the mobilized roughness component, respectively.

The second model is based on work presented by Dawson et al (cited in Krounis et al 2016) in 1998 and is given by the following expression

$$\tau_p = A_b \cdot (c + \sigma_n' \cdot \tan \emptyset_i) + (1 - A_b) \cdot \sigma_n' \cdot \tan \emptyset_b \tag{2.61}$$

Both model estimates the shear capacity by adding up the total capacity for the bonded and the unbonded parts. The only difference is that the methodology developed by Dawson et al assumes that the roughness is not mobilized prior to failure of the bond, thus they neglect the roughness component i from expression for the peak capacity. Figure 2.11 shows equation (2.60) and (2.61) plotted against various bonding rations A_b for different roughness components i.

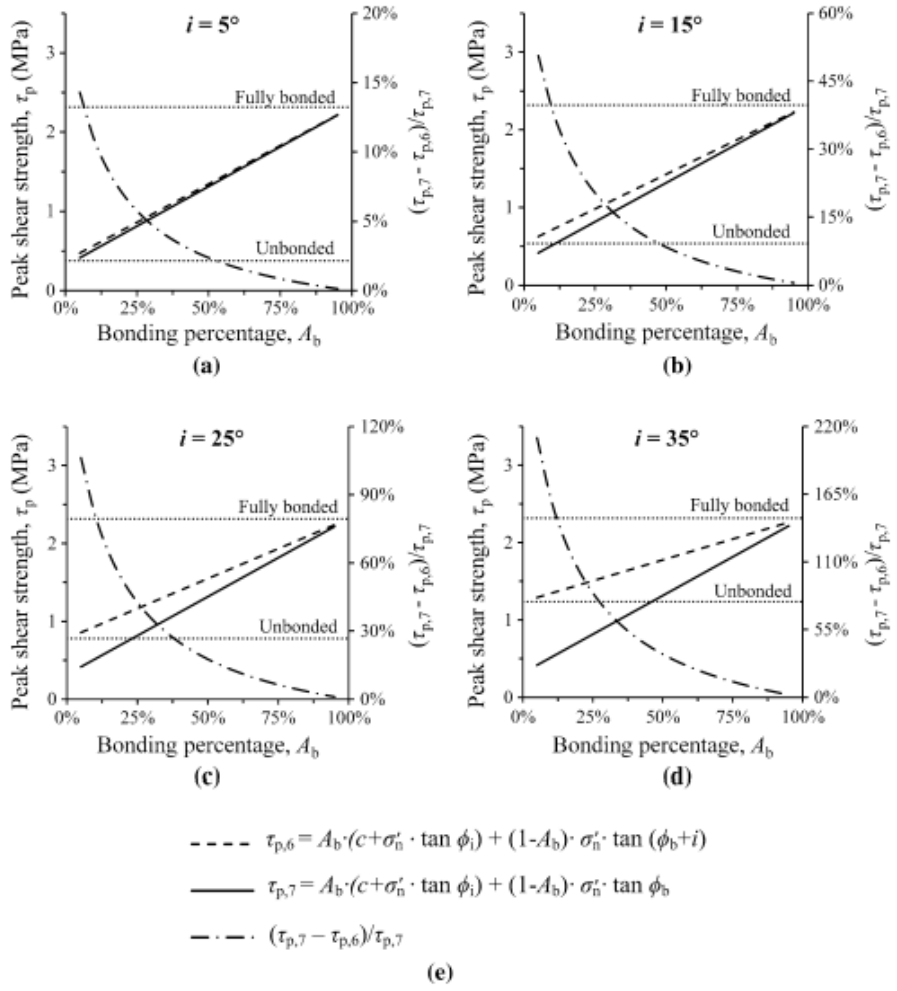

Figure 2.11: The peak shear capacity plotted against the bonding percentage for varying roughness components (From Krounis et al 2016)

The figure shows that as the bonding percentage increases the difference between the two models becomes insignificant. For lower bonding percentages, on the other hand, the deviation is higher. The authors (Krounis et al 2016) thus argued *"…that while assuming a complete mobilization of i could result in an overestimation of* τ_p*, excluding it could, in particular for rough interfaces, implies in a significant underestimation of the inferface resistance".*

To estimate the cohesion, the fully bonded specimen was tested at varying levels of normal load. The best-fit Mohr-Coulomb envelope for the peak capacity exhibited a cohesion value of 2.97 MPa and a peak friction angle of 54.4°. The rest of the unbonded and partially bonded specimen were run with a constant normal stress σ_n = 0.8 MPa. The average basic friction angle $ø_b$ = 38.6° was found from the saw-cut plane test specimen, and the average inclination

angle i = 32.7° was then found from the difference between the basic and the peak friction angle for the rough unbonded joints.

The average peak capacity was 3.20 MPa, 3.01 MPa and 3.65 MPa for bonding percentages of 75%, 50% and 25%, respectively. In comparison, the fully bonded specimen with a normal load of 0.8 MPa had an average shear capacity of 4.18 MPa, whereas the unbonded specimen had 2.58 MPa and 0.74 MPa for the rough and planar surfaces, respectively. The authors gave no direct explanation as to why the samples with 25% bonding exhibited a higher peak capacity than those with a higher degree of bonding, other than potential differences in individual surface roughness on the unbonded part of the samples. It might be that that the **degree** of bonding is not as significant for the peak capacity as the **presence** of bonding, however more tests on partially bonded joints are needed to draw any conclusions.

Interestingly, the peak capacity was reached at almost the same horizontal displacement for the fully bonded, the partially bonded and the fully unbonded rough samples. See figure 2.12 and 2.13 for typical stress-displacement curves for the different samples.

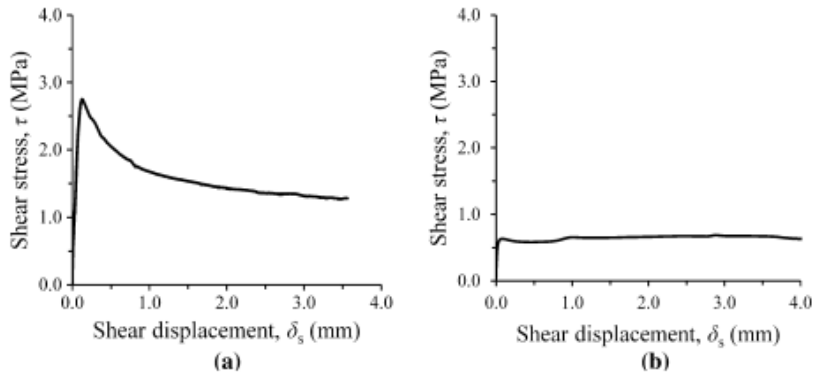

Figure 2.12: Typical stress-displacement curve for unbonded samples with (a) rough and (b) planar rock surfaces.

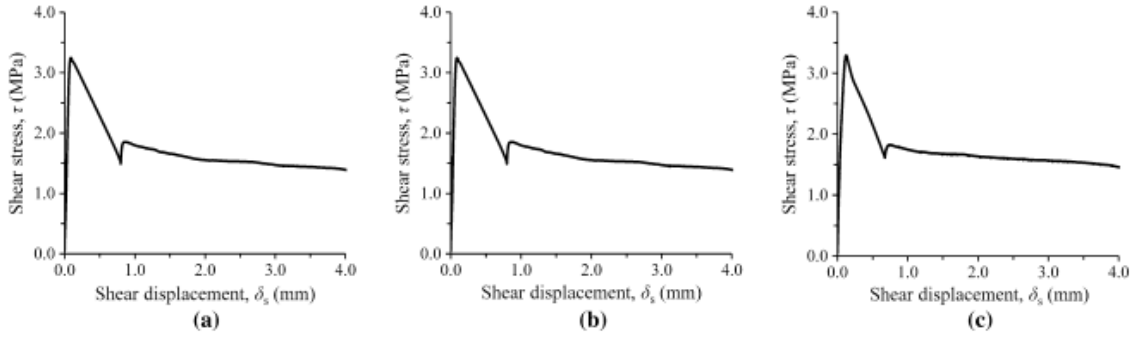

Figure 2.13: Stress-displacement curve for samples with (a) 25%, (b) 50% and (c) 75% bonding percentages.

Krounis et al (2016) consequently argued that it might be reasonable to assume that a great ratio of the roughness *i* actually can be mobilized before failure of the bond. This would favour using equation (2.60) over equation (2.61) as the former consider roughness, whereas the second does not. Plotting both models against the actual results, as done in figure 2.14, shows that equation (2.60) is a better fit than (2.59), especially as the bonding percentage decreases. The authors pointed out, however, that with a ratio of explained variance R^2 = 0.4243, neither of the models was very accurate.

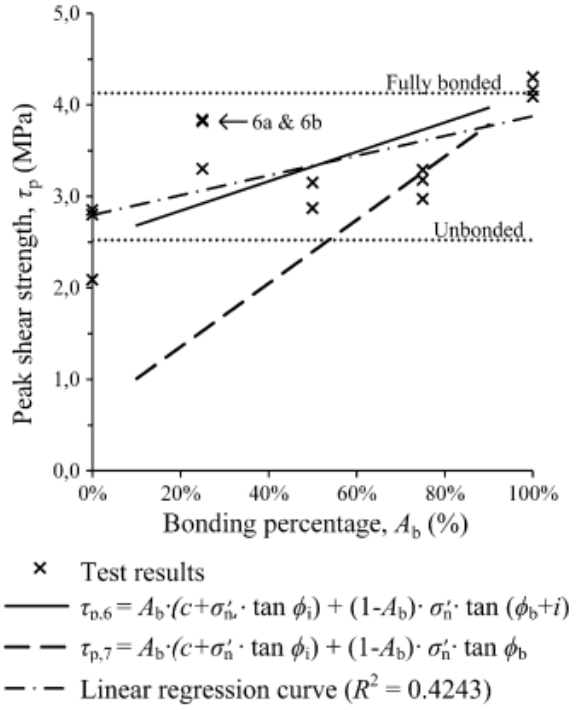

Figure 2.14: Comparison between test results and the two proposed strength models for partially bonded joints (From Krounis et al 2016).

2.3.3 Summary and Discussion

Several failure criterions have been proposed to estimate the shear strength of concrete-rock foundations. Most of them is fully or partially based on Mohr-Coulomb failure theory. As the additional cohesive *c* in the "$c + \sigma_n \cdot \tan \phi$"-Mohr-Coulomb strength envelope only is present for bonded concrete-rock joints, it is essential to distinguish between bonded and unbonded joints.

For unbonded concrete-rock joints, the peak capacity can be estimating using models from rock mechanics, describing the shear strength of rough rock joints. Patton's bilinear failure criterion is one of the most important ones. It is essentially a modified version of the Mohr-Coulomb with an added dilatational component *i*, taking the roughness into account in the expression for the friction angle. Patton recognized that as the normal load increases, the shear stress necessary to overcome the sliding resistance of the rough asperities exceeds the shear capacity of the rock, thus causing a shift in failure modes. This bilinear failure envelope is a better description of the real material behaviour than the linear Mohr-Coulomb envelope, but as Patton (1966) himself said: *"…to facilitate an understanding of the failure mechanisms curved failure envelopes reflecting the multiple modes of shear failure appear to be a necessity."*.

Ladanyi and Archambault (1969) developed a strength criterion with basis in energy considerations, however, due to the complexity of the equation, the limited experimental basis and the difficulty of defining the input parameters, the criterion did not gain wide acceptance (Donnelly and Rigbey 1998). Barton (1973) and Barton and Choubey (1977) came up with an empirical model to estimate the shear strength contribution from the joint roughness. The model take the gradual shift in failure mode into account through a dilatational expression that decreases as the normal load increases. Furthermore, the input parameters are based on numerous empirical data, and the values can be obtained from field tests. The biggest issue with this failure criterion is estimating the joint roughness coefficient accurately. Estimates from the visual comparison approach is somewhat subjective, whereas taking core samples on site and transporting them back to a laboratory for tilt tests is quite resource-demanding for quick estimations.

Grasselli (2001) used 3D-scanning to quantify the roughness of a rock profile and presented an empirical strength criterion based on the results from several shear tests. Johansson (2009) and Johansson and Stille (2014) used Grassellis scanning methodology to come up with a conceptual model for the peak capacity of unweathered rock joints based on adhesion and fractal theory. Both models make use of modern technology do accurately describe the surface roughness, however, they both rely on precise input parameters which can be hard to determine. Furthermore, they also depend on special scanning devices to map the joint morphology, which limits the use of the methodology for simple rough estimates.

For bonded concrete-rock joints, the cohesive effect from the cementitious bond becomes important for the peak shear capacity. This is especially true for joints subjected to low normal loads, as the flat slab buttress dam, where the bond strength basically determines the capacity. For higher normal loads the failure mode tends to become more of a softening failure due to the increased impact from the frictional component.

In general, it is believed that the cohesive bond is broken at small strains, whereas the dilatation and mobilization of the surface roughness require larger deformations. Hence, many authors aruge that it is not appropriate to assign a roughness contribution to the peak shear capacity of bonded joints. Donnelly et al (2007), for instance, stated that: *"It is also not theoretically possible for cohesion and the dilatational component to co-exist. Therefore roughness can not be combined with cohesive strength"*. However, the reported internal friction angle for concrete cast on natural rock profiles with bonding typically lie in the range 45°-65, whereas the basic friction angle (friction angle of a smooth surface) for concrete and rock alone is significantly lower, typically 30-40°. In addition, the test results from Tian et al (2014) with planar smooth bonded concrete-rock joints exhibited a peak friction angle of 31°, which is in the range of the expected basic friction angle. This indicates that the peak shear contribution from surfaces roughness is presented for bonded surfaces as well, but it is "concealed" in the internal friction angle of the contact $ø_i$.

Furthermore, typical concrete-rock joints as dam foundations might have a spatially distributed bonding across the interface. This was recognized by Krounis et al (2016), who performed shear tests to determine the strain-compatibility of the bonded and unbonded parts of concrete-rock samples. The results indicated that for a partially bonded joint, it might be reasonable to assume that the surface roughness component of the unbonded parts is mobilized at the same strain levels as failure of the bond.

3. Sliding Stability Analysis of Kalhovd dam

3.1 Introduction

Kalhovd dam is a flat slab buttress dam located in Rjukan, Telemark. The dam was completed in 1948 and links the two river systems Gjøystvassdraget and Mårvassdraget to the jointed reservoir Kalhovdfjorden. The total crest length is 386m, where 140m is a free spillway. The height of the dam is 15m at the most.

Figure 3.1: Kalhovd dam (Picture: Statkraft)

Due to new requirements in the Norwegian guidelines for concrete dam, the dam face major rehabilitation in the future to be considered “stable”. However, if a cohesion value can be documented and used in the stability calculations, the theoretical safety factor of the dam might increase enough to prevent an expensive restoration project. In order to estimate the potential effect of adding cohesion in the calculations, a combined dam stability analysis with both FEM and hand-calculations on one of the most critical buttresses have been carried out.

3.2 General Dam Geometry

The flat slab has a 1:0.8 inclination and rests on buttresses with a centre-centre distance of 5.0m. It is 0.3m thick at the top with an increasing thickness of 30mm per vertical meter. The buttresses have a 1:0.33 inclination on the downstream side and are 0.3m thick at the top with an increasing thickness of 22mm per vertical meters.

In addition, the dam has a vertical isolation wall on the downstream side. All of the buttresses have an opening on the inside of the isolation wall, making it possible to walk on the inside of the dam.

The dam has a free spillway over 28 section (5m each), giving a gross spillway length of 140m. The height of the walkway above the spillway is 1.12m. The abutment on both sides consists concrete gravity dams approximately 20m long.

3.3 Geometry of the Analysed Buttress

As the ice load usually become the design load for small flat slab buttress dams, one of the lowest buttresses with the lowest self-weight was chosen for the analysis. The relevant buttress is located below the spillway on the north side of the dam, and can be seen in figure 3.2. It is about 3.9m high with an approximated geometry as described in figure 3.3. To simplify the calculations the chosen buttress have nearly horizontal sliding plane.

Figure 3.2: Picture of the chosen buttress taken from inside the isolation wall.

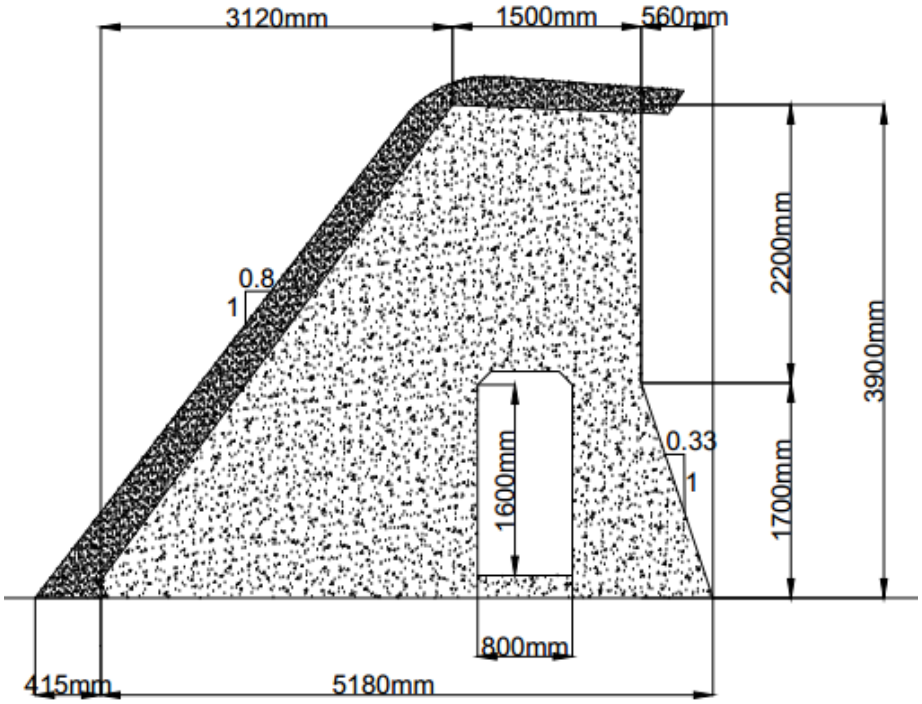

Figure 3.3: Approximated geometry and dimensions of the chosen buttress.

3.4 Finite Element Analysis

A 2D finite element analysis of the buttress described in chapter 3.3 was concducted with the FE-software Abaqus 6.14-1 made by Dassault Systèmes.

The combination of the flat slab and the buttress proved hard to model without producing artificial stress concentrations. Consequently, only the buttress was modelled and analysed. The loads applied on the buttress is equivalent to the loads transferred from a 5m long flat slab to the buttress.

As the shear strength of the rock-concrete interface highly depends on the stiffness assigned by the user, and no calibration data exist, it was decided that the finite element model only would be used to assess the stress distribution in the buttress, and not the sliding strength. The stress distribution is interesting because the shear strength of each point in the foundation interface is a function of the occurring normal stress. In addition, sufficient bonding between the concrete and the rock interface, and thus the presence of cohesion, can only be expected to occur where the tensile strength of the cement paste has not been exceeded.

3.4.1 Geometry

The geometry of the analysed buttress is approximately the same as the geometry given in 3.3. Additionally, the corresponding dam foundation was given a total length of 15m and a depth of 5 m. As the thickness of the buttress varies with depth, an average plane stress thickness of 343 mm was used for the whole model.

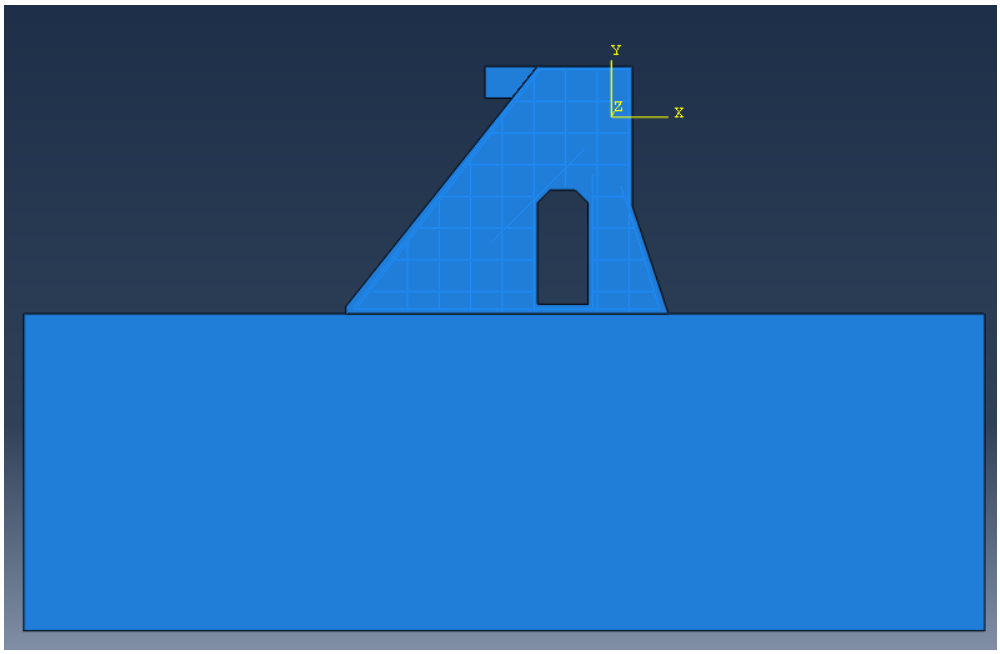

Figure 3.4: The geometry of the finite element model (From Abaqus)

The reinforcement was taken from the construction drawings provided by Statkraft (Appendix A) and embedded into the model using the constrain tool. Where the construction drawings where unclear, conservative amounts was assumed. An illustration of the amount of reinforcement used in the model can be seen in figure 3.5.

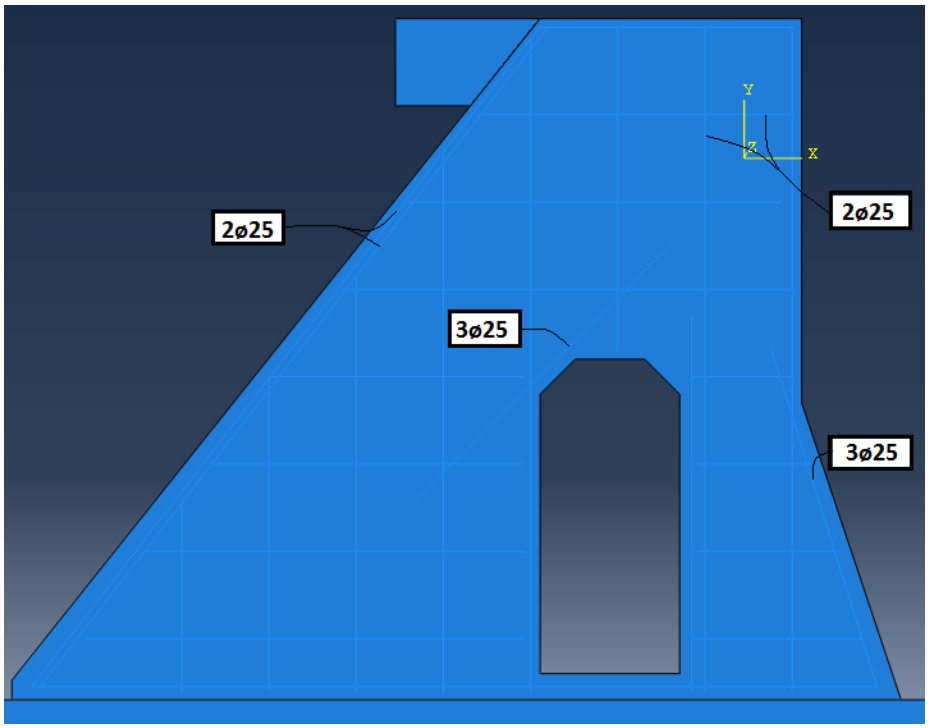

Figure 3.5: Embedded reinforcement (From Abaqus)

3.4.2 Mesh

The buttress and the rock foundation was meshed using an unstructured meshing technique with 8-node biquadratic plane stress elements and reduced integration. This element type is superior to the bilinear 4-node elements, as the quadratic shape functions can represent pure bending without displaying spurious strain and shear locking, whereas the linear cannot (Mathisen 2015). Combined, the dam and the rock foundation was modelled using approximately 30 000 elements. The reinforcement was modelled as 2D linear truss elements.

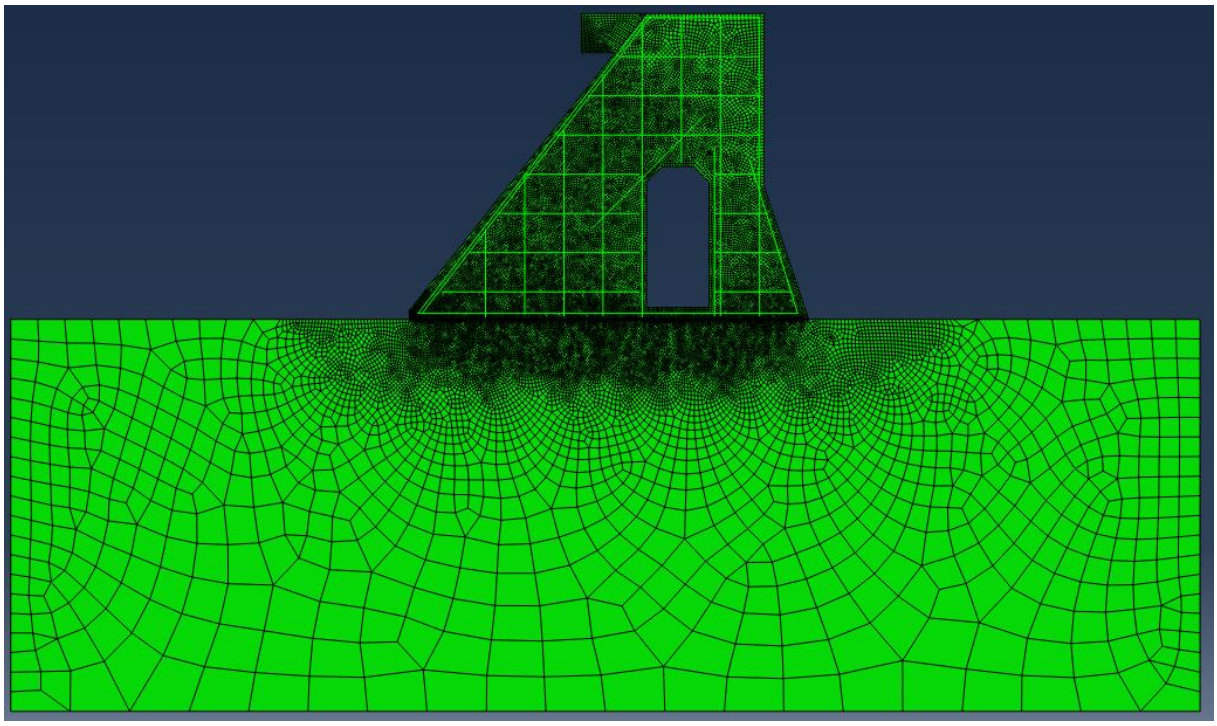

Figure 3.6: Mesh of dam and foundation (From Abaqus).

3.4.3 Contact Interaction

Abaqus differentiates between two contact formulations: node-to-surface and surface-to-surface. The contact interaction between the buttress and the rock foundation was modelled using the surface-to-surface formulation. This formulation enforces contact in an average sense over areas close to slave nodes, whereas the node-to-surface only does this at individual slave nodes, not taking into account the element thickness (Dassault Systèmes 2014).

Furthermore, the user is asked to choose between the two sliding formulations: “finite sliding” and “small sliding”. The “finite sliding” formulation accepts arbitrary separations, sliding and rotation of the surface, while for the “small sliding”, slave nodes should not slide more than one element length from the origin and still be in contact with their local tangent plane. As the main objective of the analysis was to assess the stress distribution in the buttress and not the sliding stability, “small sliding” was chosen as the sliding formulation. For surface-to-surface and “small sliding”, the penalty method is the default constraint enforcement method.

Additionally, the interface have been modelled as a “hard” contact with an additional cohesive formulation included. This contact minimizes the slave penetration into the master

surface and allows contact pressure to transmit fully the surfaces as long as there is contact (Dassault Systèmes 2014).

3.4.4 Material Models

The concrete was modelled using the "Concrete Smeared Cracking" material model. This model is designed for concrete structures subjected to monotonic straining under low confining pressures, causing the material to either crack in tensile or crush in compression (Chaudhari and Chakrabarti, 2012). The tensile cracking is presumed to be the dominating failure behaviour and the cracks are irrecoverable, however, they may open or close (Dassault Systèmes 2014). These cracks are taken into consideration independently at different integration points through a change in stress and material stiffness.

The material model uses a predefined tension-stiffening curve to describe the stress-strain behaviour after crack initiation, which allows the model to include the residual tension capacity in concrete after cracking have started. This residual capacity stems from the concrete zones laying in-between cracks and reinforcement bars still possessing some tensile strength due to their bond with the rebar.

In Statkraft Grøners (2003) reassesment report a concrete strength class of C20/25 was assumed. Using the same concrete class, the average compressive and tensile strengths was found in Eurocode 2 (2004). Furthermore, an effective Young's Modulus 20 000 MPa was assumed for the analysis.

According to the Abaqus user manual (Dassault Systèmes 2014), for well-reinforced structures, the post-cracking tension stiffening allows strains up to 10 times the failure strain before the stress is reduced to zero. Hence, the tension strain giving zero stress was set to 10 ‰ in the material model.

Combining this, the stress-strain behaviour used in the concrete material model is summarized in the bilinear model presented in figure 3.7.

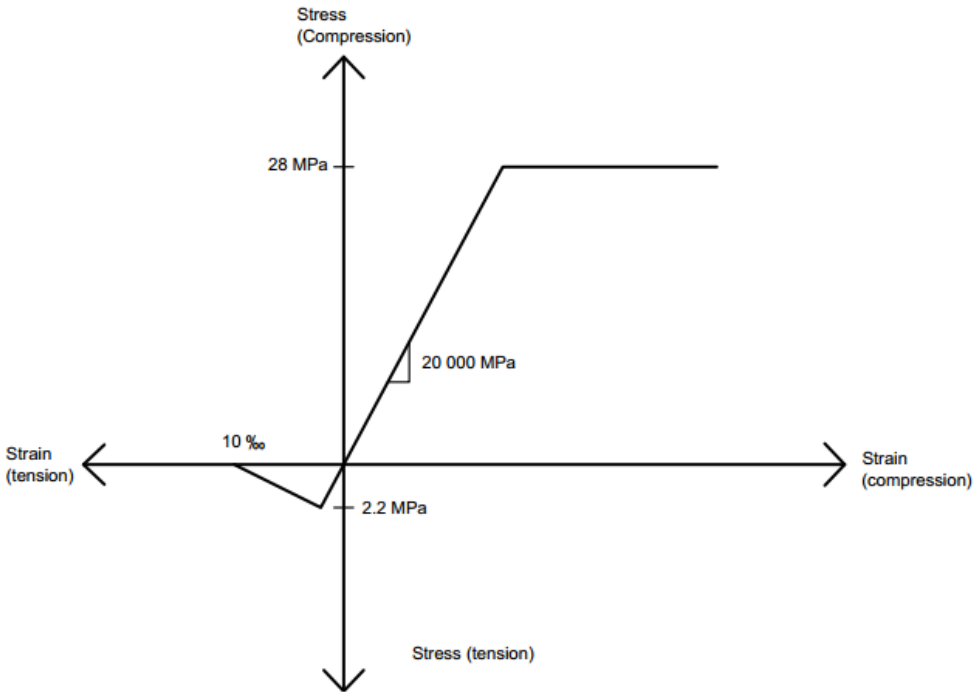

Figure 3.7: Uniaxial stress-strain behaviour for the concrete material model.

The reinforcement steel was assumed to behave elastic with Young's modulus of 200 000 MPa and perfectly plastic after the yield strength a yield strength of 220 (Statkraft Grøner 2003). The rock material was assumed to behave linear elastic with Young's modulus of 100 000 MPa.

3.4.5 Loads and Constraints

As only the buttress was modelled the loads from the flat slab was subjected to the buttress directly. An illustration of the loading and constraints conditions assumed in the model is seen in figure 3.8.

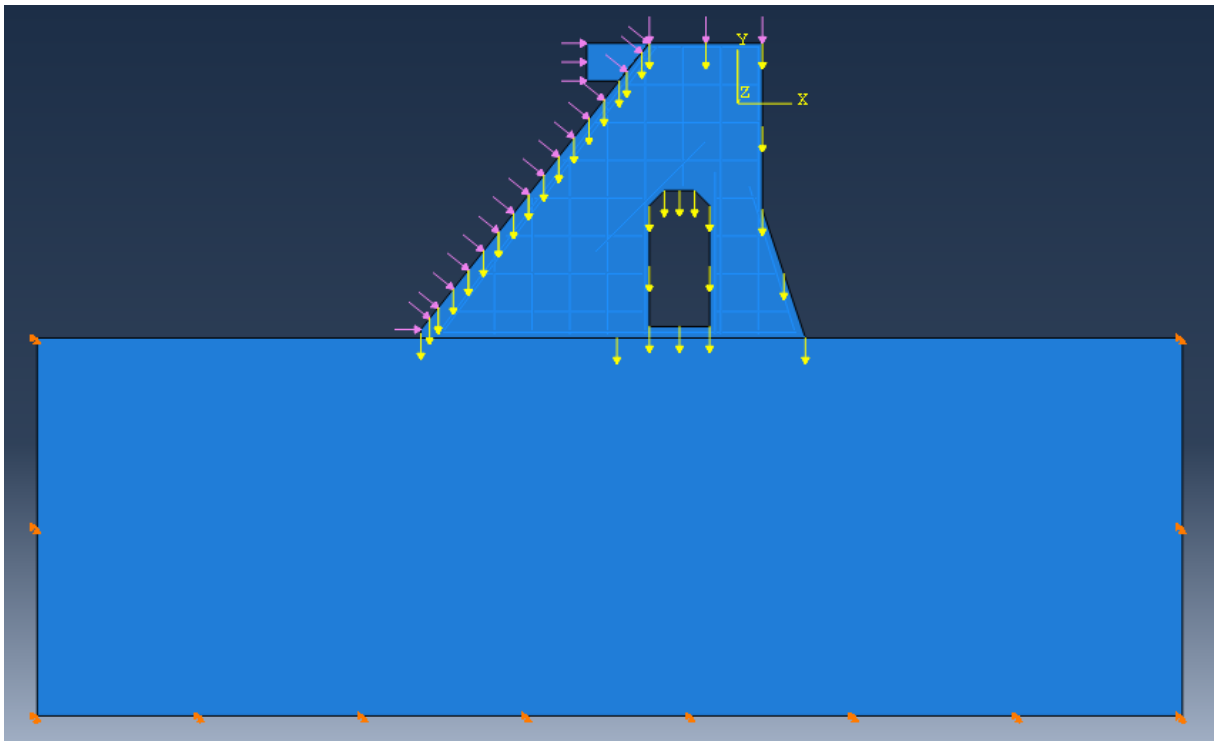

Figure 3.8: Loading and constrain for the model (From Abaqus)

The unit load of the concrete and the rock was set to 24 kN/m^3 and 28 kN/m^3, respectively. Due to limitations in load alternatives for an inclined surface, the self-weight of the slab flat was subjected to the buttress as seven vertical nodal loads on the upstream side.

Uplift from pore pressure below the slab was taken into account by a reduction in the applied self-weight of the slab. Furthermore, the self-weight of the walkway above the spillway was found from construction drawings, and applied as a constant pressure load on the top of the buttress. The ice load was modelled as a 500 mm deep rigid block connected to the crest of the buttress, subjected to a horizontal pressure equivalent to 100 kN/m.

The rock foundation was constrained against horizontal and vertical displacements at 12 of the exterior nodes.

3.4.6 Results

In this chapter, illustrations of the simulated principle stressesin the buttress, as well as the normal stresses just above the concrete-rock interface are presented.

The results from three different load cases are presented:
- Self-weight only
- Self-weight + hydrostatical load (HRWL)
- Self-weight + hydrostatical load (HRWL) + ice load

Load case: Self-weight only

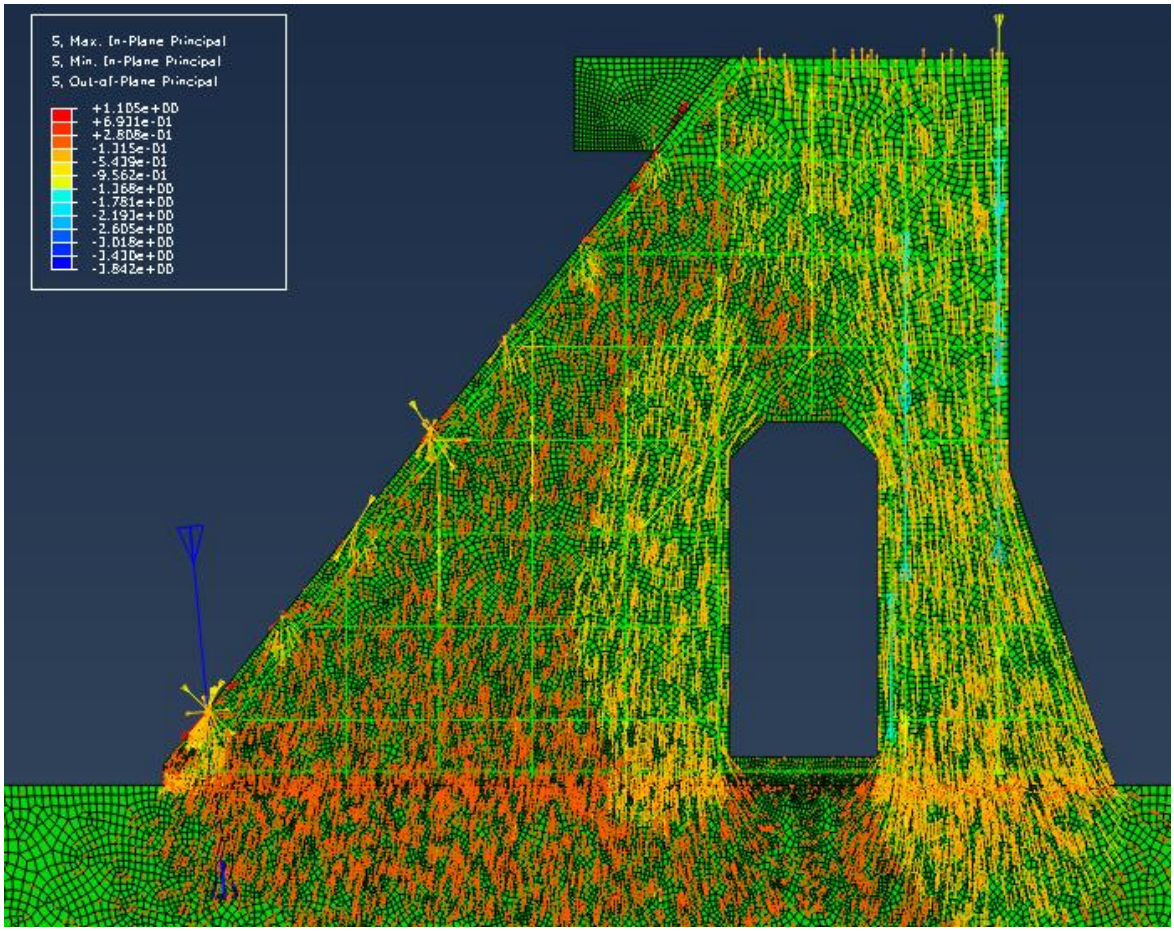

Figure 3.9: Distribution and size of principal stresses (From Abaqus).

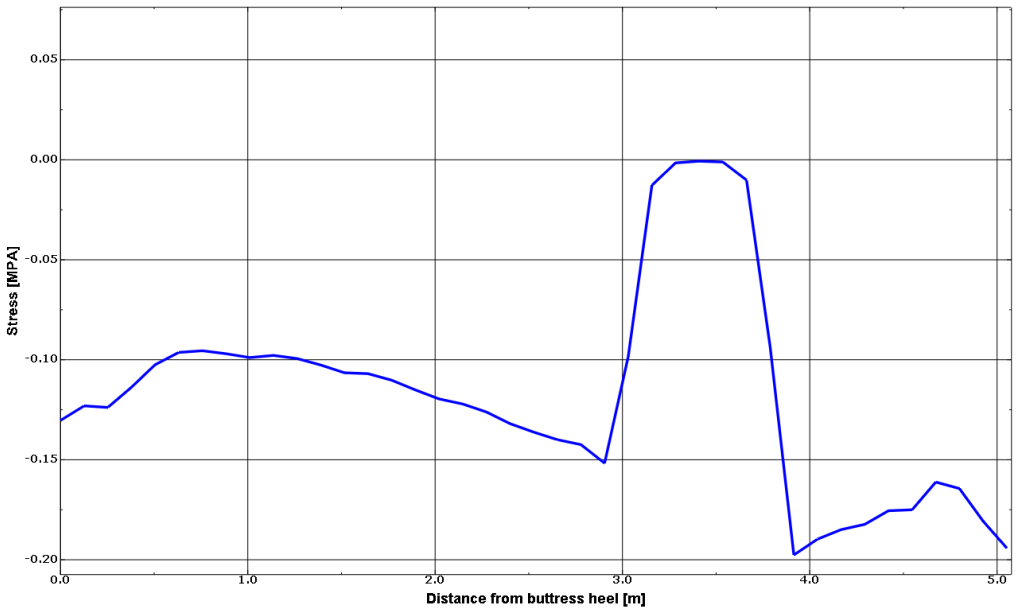

Figure 3.10: Normal stress along the foundation interface. Positive values are tension, negative compression (From Abaqus).

Load case: Self-weight + hydrostatical load (HRWL)

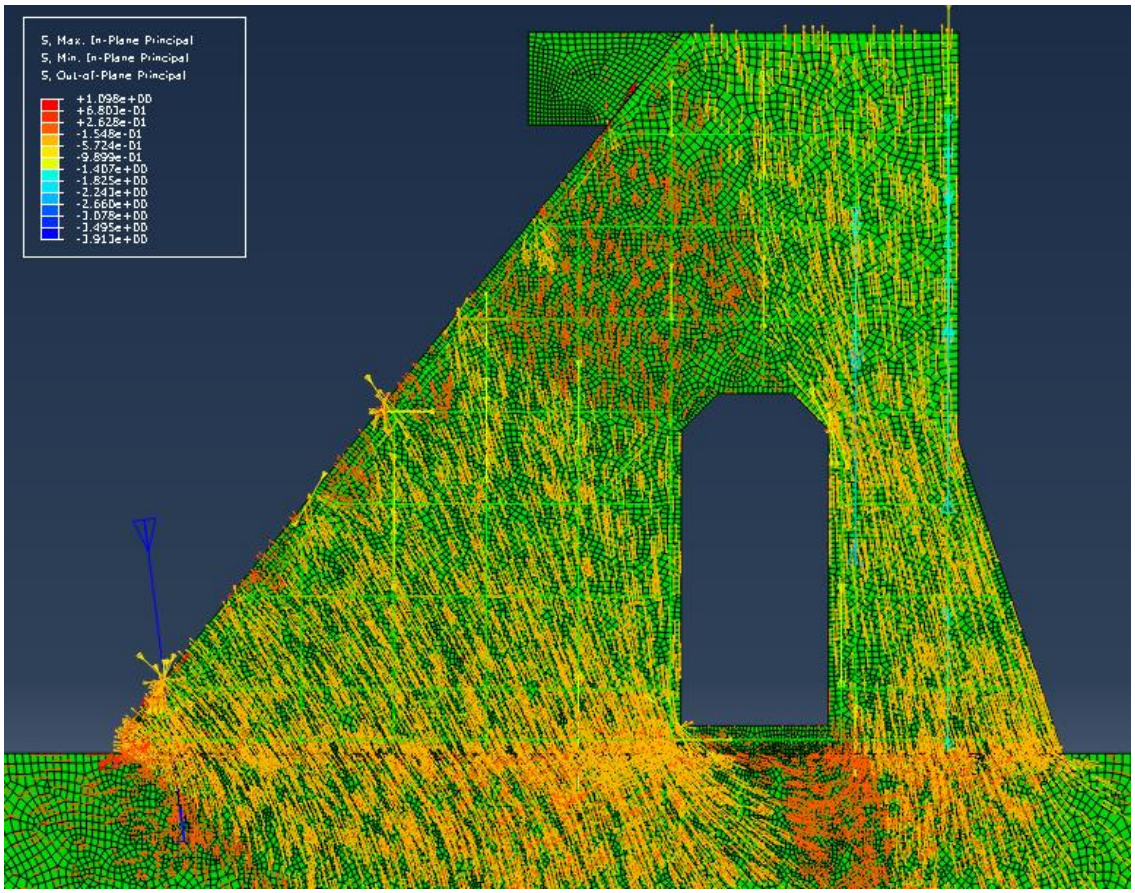

Figure 3.11: Distribution and size of principal stresses (From Abaqus).

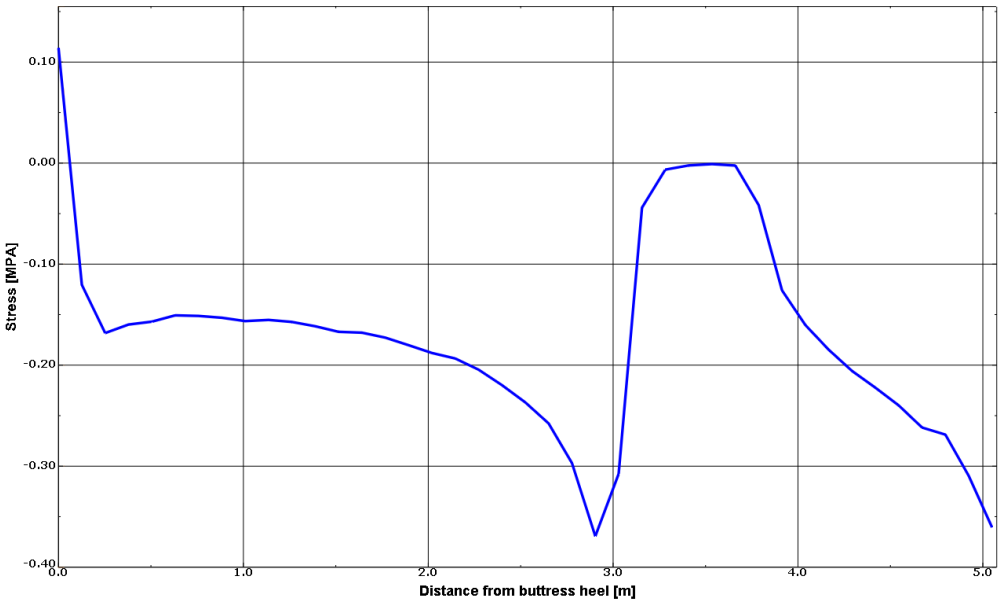

Figure 3.12: Normal stress along the foundation interface. Positive values are tension, negative compression (from Abaqus).

Load case: Self-weight + hydrostatical load (HRWL) + ice load

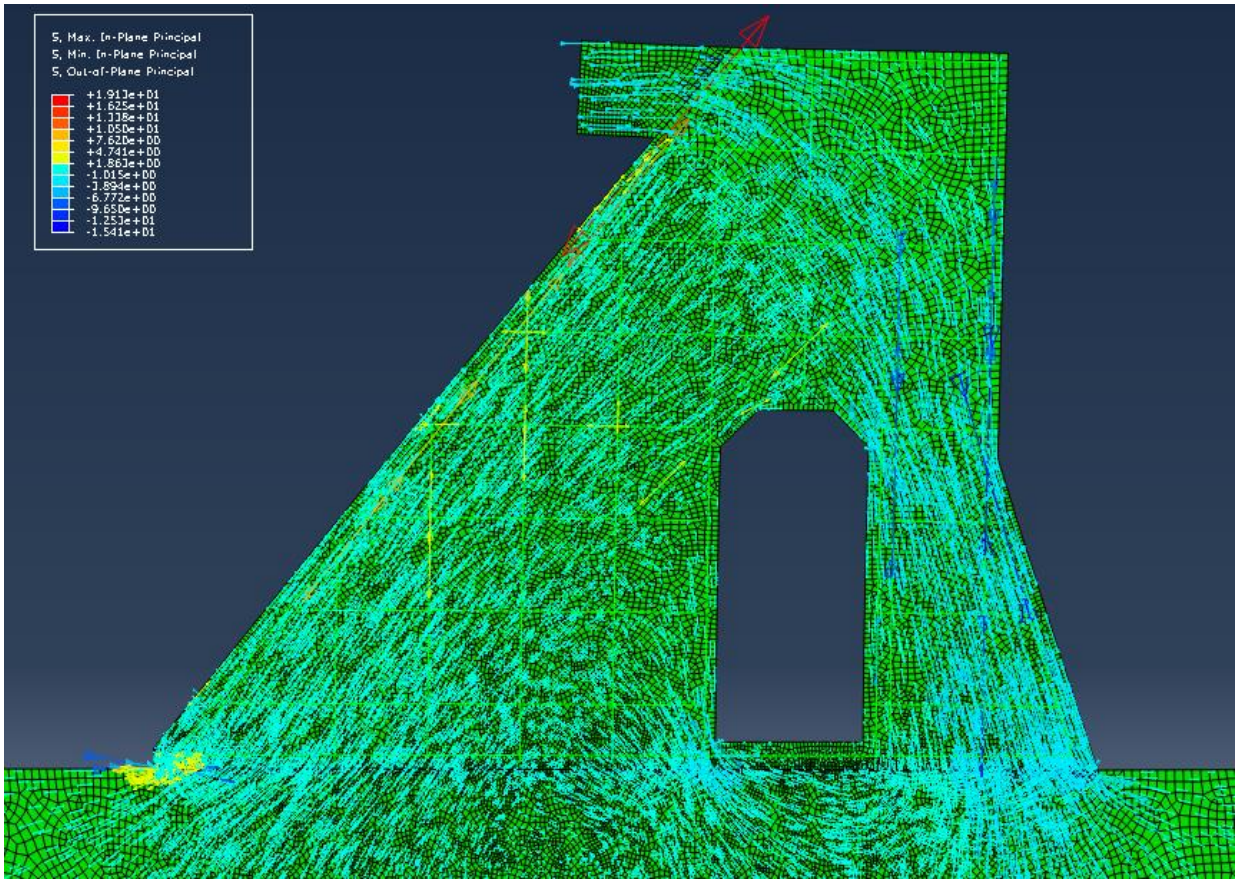

Figure 3.13: Distribution and size of principal stresses (From Abaqus).

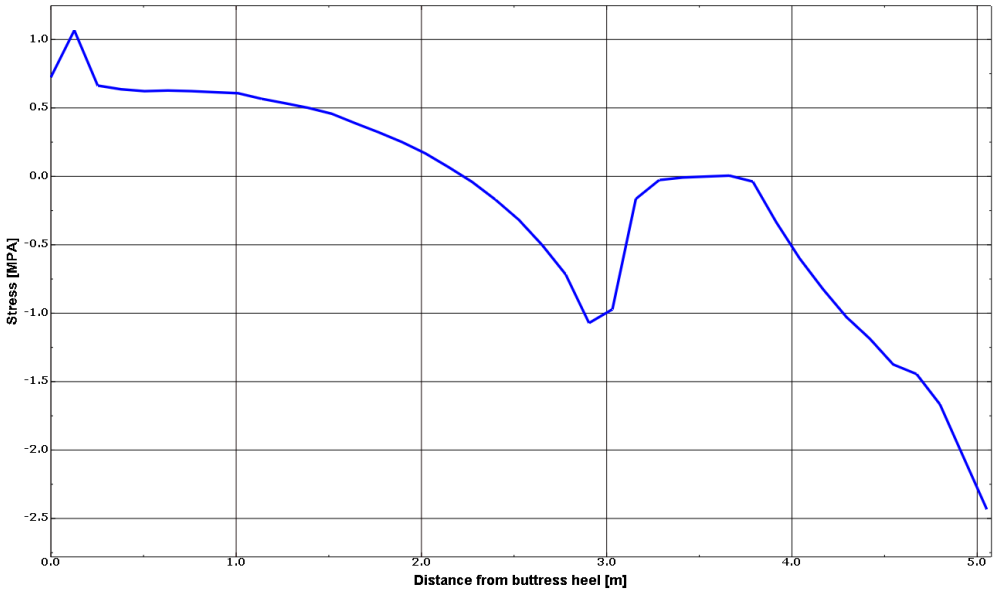

Figure 3.14: Normal stress along the foundation interface. Positive values are tension, negative compression (From Abaqus).

3.4.6 Summary and Discussion

A finite element analysis of one of the lowest buttresses on Kalhovd dam have been performed using the FE-software Abaqus, with the objective of investigating the stress distribution in the buttress. For comparison, three different load states was assessed: Self-weight only, self-weight + hydrostatical load (HRWL) and self-weight + hydrostatical load (HRWL) + ice load.

The results indicate a significant difference in the stress distribution depending on the occurring loads. For the case of self-weight only, most of the stress components is vertically oriented, distributing themselves on either side of the door opening. Furthermore, except for the area below the door opening, the whole section of the buttress is in compression in with normal stress ranging from 0.1 to 0.2 MPa.

When the hydrostatical load was applied as well, the stress components oriented themselves slightly more horizontal. The average normal stress increased somewhat in most of the foundation. However, in the first 100 to 200 mm on the upstream side, there is a sudden shift to tension stress. This shift is most likely the result of the tension stress from the overturning moment as the concrete in the heel is starting to “stretch”. A similar peak in the stress can be seen on the downstream side where the concrete is “crushed” in compression.

As seen in figure 3.13 and 3.14, the impact of the ice load is substantial. Suddenly, the major principal stresses in almost half of the buttress is in tension. The reinforcement stresses on this side increase significantly, as well. The compressive stresses on the downstream side also rises on both sides of the door opening. Furthermore, there is a clear streamline of the principal stresses from the impact area of the ice load, down into the dam toe. From the normal stress distribution in figure 3.14, it is seen that the compressive zone starts at around 2.3 m from the upstream side, which is equivalent to about 55 % of the buttress. Most of the normal stresses in this area lies in the range from 0.5 to 1.5 MPa.

From the results, it is clear that the normal stress along the bottom of the buttress is far from constant and the variation is highly nonlinear. The impact of gaps in the concrete, as for instance door openings, is also very influential for the stress distribution, especially for small buttresses. Additionally, the magnitude of the occurring normal stresses highly depend on the loads on the dam. Due to the overturning moment from the ice load, almost 50% of the

upstream foundation is in tension for this load case. This effect is, however, compensated for by a substantial increase in compression stresses on the downstream side of the dam.

This means that likewise as the normal stress, the shear capacity varies significantly along the concrete-rock interface. Consequently, averaging the shear resistance along the interface using a constant normal stress, can lead to either an overestimation or an underestimation of the real safety factor. Furthermore, as mentioned introductorily, the presence of cohesion depends on intact bonding between the concrete and the rock foundation. However, with tension stress in a part of the dam foundation, the tensile capacity of the cement paste that binds the concrete and the rock together might have been exceeded. The result is crack propagating through the tensile zone and degradation of the bond. As the tensile strength of the cement mortar cannot be determined with high certainty, a conservative assumption is to neglect cohesion completely in the part of the dams experiencing tension during the most critical load combination.

3.5 Sliding Stability Analysis: Norwegian Guidelines

3.5.1 Criterion and input parameters

In order to assess the effect of using cohesion a sliding stability analysis have been carried out according to the stability criterion given in the Norwegian Guidelines for Concrete Dams (NVE 2005) produced the Norwegian Water and Energy Directory (NVE). The criterion is derived from the shear friction method combined with the Mohr-Coulomb criterion, and for a horizontal sliding plane, it has the following form:

$$FS = \frac{c \cdot \mathrm{A}_{comp} + \sum V \cdot \tan \phi_i}{\sum H} \tag{3.1}$$

where FS is the factor of safety, c is the cohesion, A_{comp} is the area of the dam in compression, $\sum V$ is the sum of the vertical forces including uplift, $\sum H$ is the sum of the horizontal forces and ϕ_i is the internal friction angle of the contact.

Cohesion can only be used in the stability calculations if the value can be documented. Additionally, if cohesion is used in the calculations, a higher safety factor *FS* is required. A summary of the required safety factors is given in the table below:

Table 3.1: The necessary factor of safety against sliding for flat-slab buttress dams according to the guidelines from NVE (2006).

Load case	**Cohesion documented**	**Factor of safety *FS***
Design loads	No	1.4
	Yes	2.5
Accidental loads	No	1.1
	Yes	1.5

The guidelines allows the use of rock bolts in dam stability calculations for dam sections lower than 7 m. However, the maximum bolt stress should be set to 180 MPa and one of the rock bolts should be considered inactive in every section considered. Furthermore, according to an amendment to the guidelines (NVE 2012), if rock bolts are used in the stability calculations, an additional control of the stability must be performed for the load case with

design flood level (DFL), without including the contribution from rock bolts. For this case, the minimum safety factor should be set to 1.1. The construction drawings (see Appendix A) are unclear whether rock bolts are present, so the calculations have been done both with and without ø25 rock bolts, with a centre-to-centre distance of 1000mm, included in the bottom of the slab.

The friction angle $ø_i$ has been set to 50°, which is the maximum allowable value given in the guidelines (NVE 2005) for hard rocks with rough surfaces and favourable cleavability in the concrete-rock interface. The guidelines further state that cohesion can only be included in the interface area experiencing compression, though, how the compressive zone should be found is not explained. The compressive zone of the foundation interface is therefore assumed to be 55 % of the total area in accordance with the results from the FE-analysis in chapter 3.4. Furthermore, to simplify the calculations, an average buttress thickness of 343 mm have been assumed when calculating the self-weight of the buttress. The buttress was assumed to take up water, ice and self-load from a five-meter section of the flat-slab.

3.5.2 Results

The calculations have been done for three load combinations:
- Highest regulated water level (HRWL) with an ice load of 100kN
- Design flood level (DFL), which is 0.92m above the crest of the spillway.
- Maximum flood level (MFL), which is 1.63m above the crest of the spillway (Accidental load).

Calculated safety factors both with and without rock bolts and cohesion included in the calculations:

Table 3.2: Calculated safety factor for different load cases.

Variables		Calculated factor of safety *FS*			
Rock bolts	**Cohesion value *c* [MPa]**	**HRWL and ice load**	**DFL**	**Check: DFL without bolts**	**MFL**
Not included	Not included	0.85	1.60	-	1.44
Not included	1.32	2.50	4.20	-	3.53
Included	Not included	1.33	2.35	OK	2.04
Included	0.94	2.51	4.20	OK	3.53

3.5.3 Discussion

The results shows that all the calculated safety factors fulfils the requirements from NVE for all load cases expect for the load case with HRWL and ice load. For this load case the sliding capacity does not meet the necessary requirements given in the Norwegian guidelines for concrete dams, even with rock bolts included. For the instance with neither cohesion nor rock bolts included, the calculated safety factor was as low as 0.85. The necessary cohesion value to fulfil the requirements was 0.94 MPa if rock bolts were included in the calculations and 1.32 MPa if they were not. This is within the cohesion values reported by for instance EPRI (1992), suggesting that being allowed to use cohesion in the stability calculations might bring the dam within the requirements from NVE.

One problem that arises when applying cohesion in sliding stability calculations is that the guidelines only allows the engineer to assume a cohesive strength in the compressive zone of the dam. This is not a problem for concrete gravity dams, as the compressive strains usually are so small that linear elastic beam theory is valid, and thus a linearly varying normal stress distribution can be assumed (Guttormsen 2013). However, for flat-slab buttress dams with a higher utilization of the concrete compressive strength, linearity might not always be the case. Moreover, irregularities in the geometry, as for instance door openings, will also affect the stress distribution significantly, especially for small buttresses.

By assuming a linearly varying normal stress, the compressive zone was estimated to be 4.49 m using simple hand calculations (see Appendix D). This is equivalent to 87 % of the total interface area, which is considerably more than the 55 % found from the FE-analysis in chapter 3.4. Consequently, using linearly varying normal stresses might overestimate the actual compressive zone extensively. Although very time consuming, finite element modelling seems like a more reliable tool for this purpose than old-fashioned hand calculations. One of the other advantages with using FE-analysis is that the results also gives the analyst a very clear overview of the general stress distribution in the dam.

Another method to estimate the compression zone might be systematic core drilling along the length of several buttresses, to visually inspect where the concrete-rock interface no longer are bonded. This method is, however, quite time- and resource-demanding and could in worst-case damage the buttresses

3.6 Sliding Stability Analysis: JRC-JCS model

3.6.1 Criterion and input parameters

To investigate the effects from surface roughness, stability calculations have been done using the failure criterion introduced by Barton (1973) and Barton and Choubey (1977). In order to compare the results with the results from chapter 3.5.1 an expression for the factor of safety FS of the rock-concrete interface have been derived by combining the shear friction model and the JRC-JCS strength criteria (see Appendix B for derivation):

$$FS = \frac{\sum V \cdot \tan\left(JRC \cdot log_{10}\left[\frac{JCS}{\sigma_n'}\right] + \phi_r\right)}{\sum H} \tag{3.2}$$

where $\sum V$ is the sum of the vertical forces, JRC is the joint roughness coefficient, JCS is joint wall compressive strength, σ_n' is the effective normal stresses and ϕ_r is the residual friction angle.

As the JRC-JCS model is based on the shear strength of non-intact rough rock joints, it is not appropriate to assign a cohesion contribution to the sliding resistance. Thus, the sliding model expressed by equation (3.2) assumes no bonding between concrete and rock, and that the shear capacity of the concrete-rock interface resembles the shear capacity of a rough rock-rock interface. For most cases, the compressive strength of concrete is far lower than the compressive strength of rock. Hence, the concrete compressive strength becomes the critical parameter for the sliding failure, and the JCS-value should be determined accordingly. For this analysis, the JCS was set to 28 MPa, which is consistent with the average compressive strength given in Eurocode 2 (2004) for concrete class C20/25.

During field inspections in February 2016 the bedrock of the dam foundation was found to be in overall good condition. The rock exhibited little to no signs of weathering. Consequently, it could an be assumed that the residual friction angle $\emptyset_r$ is equivalent to the basic friction angle $\emptyset_b$. According to the national bedrock database provided by the Geological Survey of Norway (Geo.ngu.no 2016) the rock type at the dam site is mylonite. However, finding tabulated values of $\emptyset_b$ for this rock type proved difficult. Thus, a basic friction angle of 30° was assumed for the analysis.

Furthermore, the investigations showed a substantially rough interface. A comparison of the in-situ roughness with the roughness profiles from Barton and Choubey (1977) can be seen in figure 3.15. From the comparison, a subjective JRC-value of 15 was chosen for the analysis.

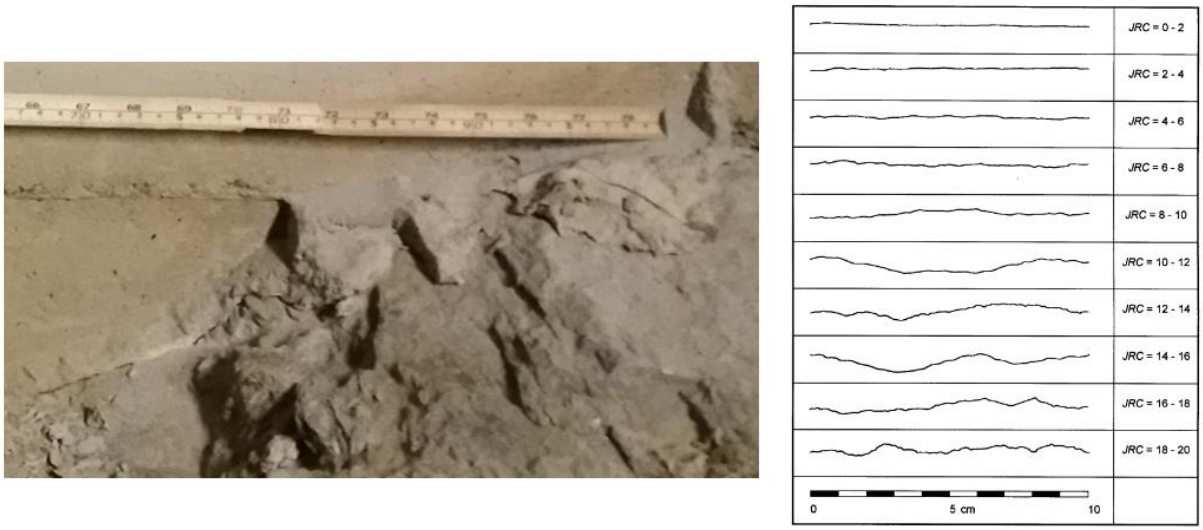

Figure 3.15: Comparison of in-situ roughness with roughness profiles provided by Barton and Choubey (1977).

3.6.2 Results

The calculations have been done for three load combinations:
- Highest regulated water level (HRWL) with an ice load of 100kN
- Design flood level (DFL), which is 0.92m above the crest of the spillway.
- Maximum flood level (MFL), which is 1.63m above the crest of the spillway (Accidental load).

Calculated safety factors using both with and without rock bolts included:

Table 3.3: **Calculated safety factors for different load cases using the JRC-JCS model.**

Variables		**Calculated factor of safety *FS***			
Rock bolts	**Roughness contribution *i* [°]**	**HRWL and ice load**	**DFL**	**Check: DFL without bolts**	**MFL**
Not included	29	1.20	2.25	-	2.04
Included	29	1.87	3.32	OK	2.89

3.6.3 Discussion

Likewise as the results from chapter 3.5.2, HRWL and ice load was the only critical load combination. The results shows that the calculated safety factor *FS* is sufficient if rock bolts are included in the calculations. For the case without rock bolts, the calculated factor of safety was 1.20, which is considerably higher than the one found from chapter 3.5.1 (*FS* = 0.85) without rock bolts and cohesion included. It should be pointed out, though, that the calculated safety factor highly depend on the initial assumptions made for the input parameters. Especially the subjectively selected joint roughness coefficient JRC have a high impact on the results. Nevertheless, it is interesting to see that another method considering the actual roughness of the dam site might give an adequate factor of safety, even when leaving out cohesion completely.

It is in the author's belief that if cohesion cannot be included in sliding stability calculations, the use of a higher friction angle should be allowed if it can be documented properly. The JRC-JCS model could be a good option for this, especially if the JRC-value and the friction angle is back calculated from tilt tests on core samples from site, and the JCS-value is found from compressive strength tests on concrete samples from the dam.

4. Development of Test Methodology to Document Cohesion

4.1 Introduction

As mentioned in chapter 3, the Norwegian guidelines for concrete dams (2005) does not permit the use of cohesion in sliding stability assessments unless cohesion can be documented through tests. However, the guidelines give no explanation of how these tests can be performed, leaving many consultants and dam owners frustrated. The purpose of this chapter is to come up with a practical test methodology to estimate the cohesion value, primarily for flat-slab buttress dams casted on bedrock.

4.2 Requirements

In order for the methodology to implementable as a standardized routine for documenting cohesion, the test procedure should fulfil certain requirements. Firstly, the methodology must be able to represent the real conditions at the dam site of interest. Preferably, the actual roughness and strength of the bedrock should be taken into account. Secondly, it must be feasible to use at different dam sites without requiring rare and very expensive equipment. The method must be scientifically acceptable and represent the correct failure mechanisms behind a sliding failure. Artificially introduced stress and should be avoided or kept to a bare minimum. Furthermore, the results from the testing should be accurate and reliable enough to use in dam stability calculations.

4.3 Preliminary Testing of a Methodology

In order to propose a test methodology that is as practical and viable as possible, a preliminary method was developed and tested. The initial method was developed through discussions with senior engineer Odd Kristian Nerdahl at NTNUs structural lab, professor Leif Lia at the department of Hydraulic and Environmental Engineering, and Harald Andreas Simonsen and Rolv Guddal from Statkraft and Sira-Kvina, respectively.

4.3.1 Preparing the Samples

In total six circular core samples of rock with a diameter of 150 mm were drilled at two different sites. Neither of them represent the rock quality at a given dam, but as the intention only was to test the methodology, any rock worked fine.

Figure 4.1: Example of drilled core samples

The samples were then transported to Trondheim, and cut into cubes approximately 100x100x100 mm, at the Department of Geology and Mineral Resources Engineering, leaving the original surface intact.

Figure 4.2: Cutting the core samples into cubes

The samples were then placed pairwise into pre-cut formwork boxes, with the original surfaces facing each other, as shown in figure 4.3. Due to the limited accuracy of the rock

saw, the dimensions of the cubic samples was somewhat smaller than the dimensions of the formwork boxes (95x95 mm instead of 100x100), leaving a small gap between some of the rock samples and the sides. This problem was solved by putting a thin wood sheet in-between the test-specimen and one of the sides of the box. This was sufficient enough to cast the samples, but unfortunately it made some of the concrete surfaces slightly uneven.

In order to ensure a sufficient early compressive strength after only 5 days of curing, a concrete mixture with a rather low water-cement ratio was chosen. The chosen concrete mixture was taken from a table proposed by Kosmatka and Wilson (2011) for small jobs, and had water/cement-ratio of 0.4.

Table 4.1: Concrete mixture recipe proposed by Kosmatka and Wilson (2011).

Ingredient	**Quantity**
Cement	400 kg/m^3
Fine aggregate	670 kg/m^3
Coarse aggregate	1040 kg/m^3
Water	160 kg/m^3

Figure 4.3: Casting of test samples

In total three test-specimen were cast. After casting, the test samples were covered with a plastic sheet to prevent moisture loss and left to cure at a constant room temperature for five days.

4.3.2 Testing the Samples

The shear strength of the test-specimens were tested at one of the electromechanical testing rigs at the structural lab at NTNU. The rig is a high precision screw-driven testing machine with a maximum thrust force of 100kN. This machine was preferred over the larger hydraulic driven test rigs, which might be subjected to unstable loading conditions for brittle material failures.

Figure 4.4: The electromechanical testing rig.

The test specimen were placed on two steel plates, leaving only a gap for the concrete part to slide through. To limit the acting moment and thereby the bending effects, the plates were placed as close to the rock-concrete transition zone as possible. Furthermore, normal stress was applied by mounted two vertical steel plates on each of the short sides of the sample and connecting them with threaded bars and nuts. The normal stress was then continually logged by a load cell placed in-between one of the vertical steel plates and the test-specimen. A steel plate was placed at the top of the concrete section to transfer the load as evenly as possible

down into the concrete section. The test machine then recorded vertical force and displacement continually as the test was running. Figure 4.5 shows the setup of the shear tests.

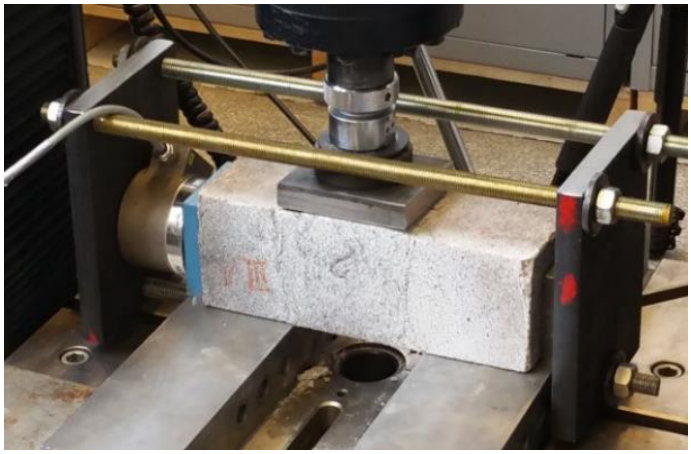

Figure 4.5: Setup of the shear test at the test rig.

The samples were first preloaded until sufficient contact between the steel plate and the concrete was achieved. The tests was then run from this state as a reference point with a constant displacement of 0.20 mm/min until the end.

Originally, the three tests were originally planned to run with a constant normal stress of 0.3, 0.6 and 0.8. However, due to irregularities in the surface roughness, the normal load of the first test kept increasing as the vertical deformations became larger. Thus, it was evident that holding the normal stress constant would be difficult. Consequently, in an attempt to reduce the incurred normal load as much as possible, the next two tests were loaded enough to only keep the load cell tight.

4.3.3 Results

Shear test I:

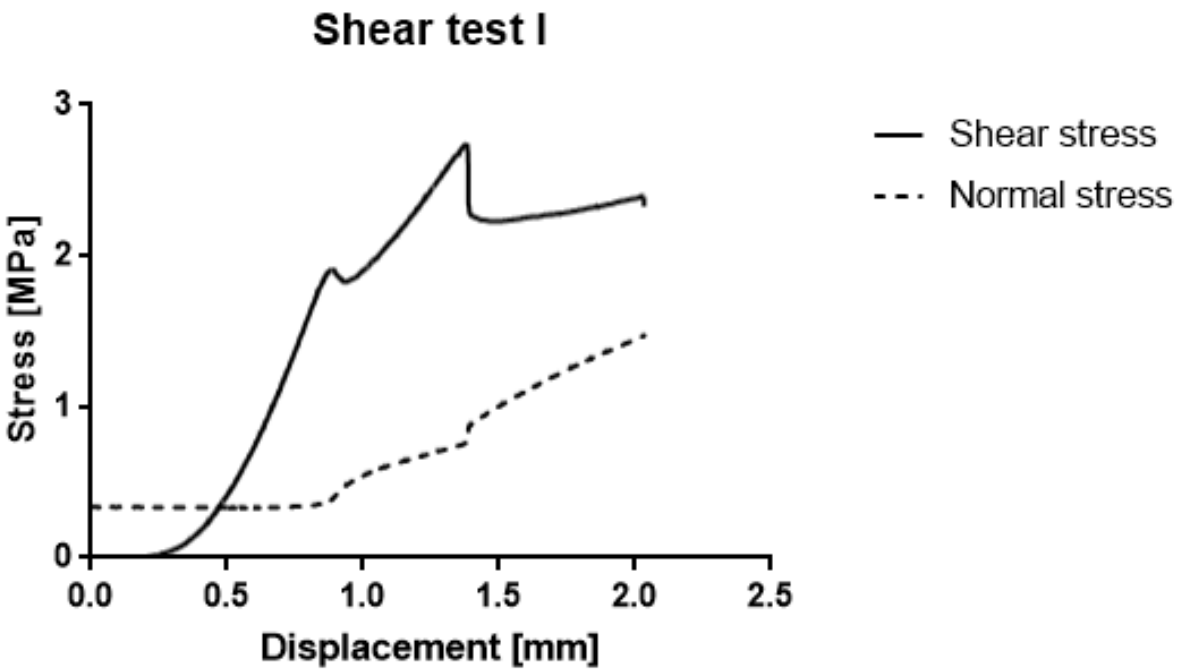

Figure 4.6: Shear and normal stress plotted against displacement for** test **I.

Figure 4.7: Test sample I after failure.

Shear test II:

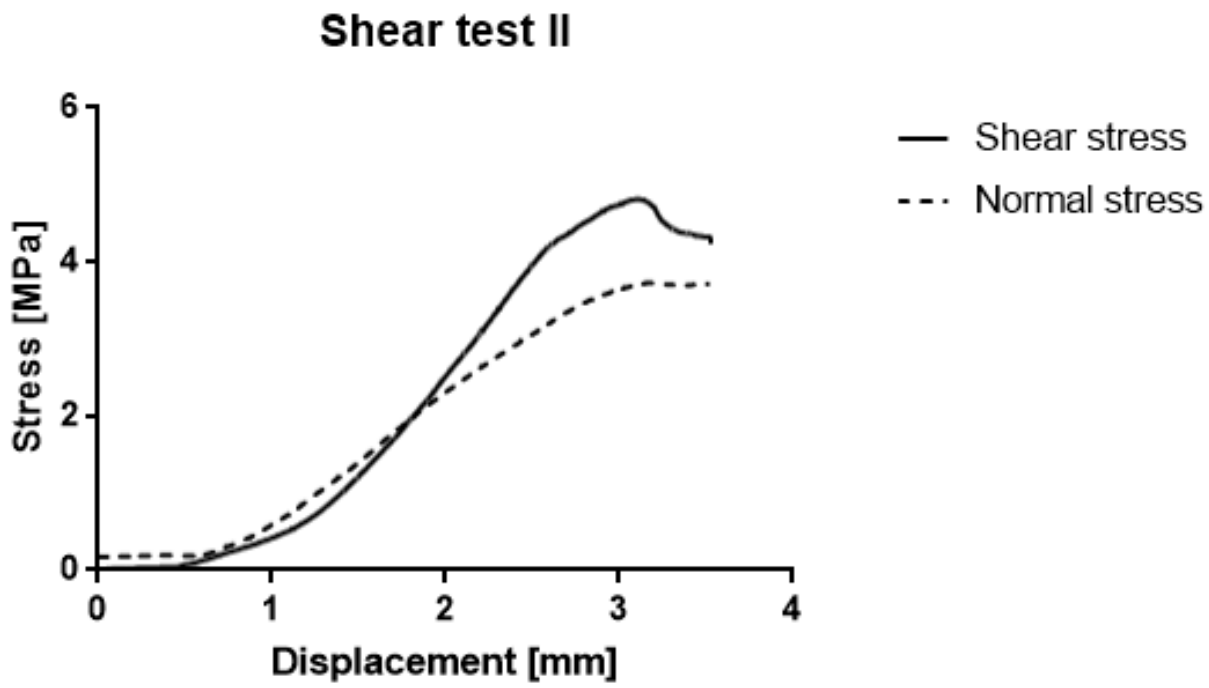

Figure 4.8: Shear and normal stress plotted against displacement for test II.

Figure 4.9: Test sample II after failure.

Shear test III:

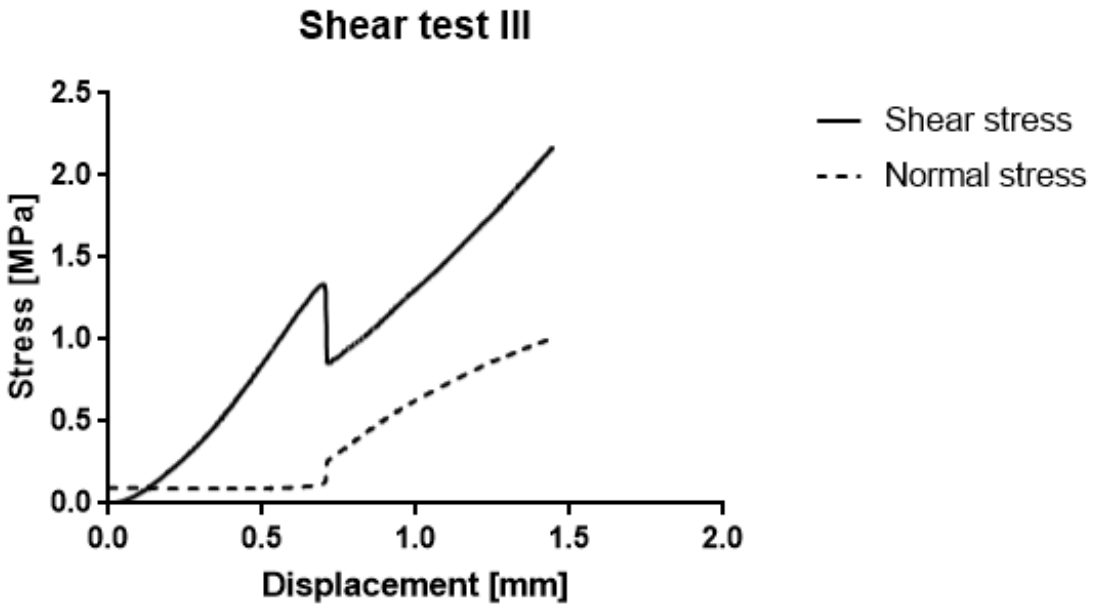

Figure 4.10: Shear and normal stress plotted against displacement for test III

Figure 4.11: Test sample III after failure.

4.3.4 Discussion

Shear test number I was preloaded with a normal force of 3.06 kN, corresponding to a normal stress of approximately 3.33 MPa. The τ-σ-curve exhibits typical shear behaviour until a small peak is reached at a shear stress of roughly 1.9 MPa, before the shear stress increases again. This first peak is believed to be caused by a defect in the rock surface reaching its capacity. Visual inspections afterwards supports this theory, indicating a small popout on one of the rock surfaces, as seen in figure 4.12. The second peak and maximum capacity is reached at a shear stress $\tau = 2.74$ MPa. Here there is a significant reduction in capacity, typically associated with a complete failure of the bond.

Figure 4.12: Rock defect in shear test I

The normal stress was practically constant until the first peak of the curve is reached, giving a sudden increase from about 0.40 to 0.55 MPa. After this, σ increased slowly to roughly 0.76 MPa at the second peak, before suddenly leaping up to 0.86 MPa after the bond failed. This sudden increase in normal stress at the peaks is believed to be triggered by the brittle failure mechanism when the bond is degraded, which causes a small slip and mobilization of the surface roughness in friction. This is in line with the findings by Moradian et al (2011, 2012) suggesting that for low normal loads, the roughness of the asperities are not utilized before after the bond has failed.

It is believed that as soon as the rock defect fails, the lower part of the interface is mobilized in friction, leading to the small increase in normal stress between the peaks. After the bond is completely degraded at the second peak, both interface is mobilized in pure friction. As the deformations increase, more of the roughness is mobilized, thus increasing the normal stress even more. It is this rise in normal stress, which leads to the seemingly increase in residual capacity after degradation of the bond. In addition, as figure 4.7 shows, both joints tend to

incline somewhat to one of the sides. This effect most likely intensified the rise in the normal force even more.

Shear test number II was preloaded with a normal stress of roughly 0.18 MPa. In contrast to the results from test I, the normal stress started to increase simultaneously with the shear stress. Consequently, the normal stress was almost the same as the shear stress at the point of failure, resulting in a gradually frictional failure instead of the more brittle bond failure. The reason for this peculiar shear behaviour is believed to stem from the preparation of the samples. Due to limitations on the accuracy on the cutting machine, the rock samples was not completely identical, resulting in sides that were not aligned entirely perfect. Hence, significant bending action had to be introduced, before both of the bottom sides were in fully contact with the underlying steel plates, and shear deformations could start. This effect is demonstrated in figure 4.13, which shows the mounting of test sample II before and after the shear test was carried out. Therefore, it is reasonable to assume that the introduction of bending stress contribute significantly to the early rise in normal stress seen in figure 4.8.

Figure 4.13: Mounting of test sample II before (over) and after (below) the shear test.

In the end, test number II reached a peak shear capacity of 4.81 MPa with a normal stress of 3.72 MPa. However, the introduction of artificial bending stress makes the result highly questionable.

Shear test number III was given an initial normal stress of around 0.1 MPa. This normal stress remained nearly the same until failure of the bond at $\tau = 1.32$ MPa, which triggered a sudden rise similar to test I. For this test, however, only the lower part on one of the joints failed. The reason for this is most likely the somewhat uneven loading surface on the concrete of this

specimen seen in figure 4.11, which failed to distribute the stress evenly. After the brittle failure on the lower part, the crack started propagating into the concrete section. This further indicates that the outer part of the loading plate probably was not in sufficient contact with the concrete to the transfer load properly.

Interestingly, the normal stress for this test behaved similarly to the normal stress in test I; it remained stable until failure of bond, where it started to rise. This further strengthens the theory that the roughness is not utilized before after degradation of the bond. Nonetheless, the irregular failure mechanism of this test-specimen makes it difficult to draw any certain conclusion from the results, other than a general underlining of the importance of using well-prepared test-specimen.

4.4 Proposed Test Methodology

The proposed test methodology is mainly based on the methodology given in the section before. Some adjustments have been made after studying the results from the preliminary testing and discussing with engineer Steinar Seehuus at the structural lab.

4.4.1 Verifying Bonding

In order for a concrete dam to have a cohesive sliding resistance, a sufficient bond between the concrete and the rock foundation must be present. Before any cohesion tests are carried out, bonding should be verified in an adequate number of buttresses. In a meeting 27.01.2016 between Harald Andreas Simonsen (Statkraft), Ronald Andersen (NVE) and Rune Engesæter (NVE) it was mentioned that checking 10 % of the buttresses of a dam would be acceptable for this matter (Simonsen H.A., Personal Communication, 07.06.2016). The bonding can be verified by core drilling through the buttresses on the downstream side of the dam and visually inspecting the concrete-rock interface on the drilled samples.

4.4.2 Extraction and Preparation of Test Specimen

Circular core samples with a dimeter of 150 mm are extracted at dam the site. The samples should be approximately 120-150 mm long and the surface roughness of the samples should be representable for the surface roughness of the dam foundation. Furthermore, to minimize the incurred normal stress during testing, the samples should be extracted from an area with as low inclination as possible. Alternatively, if no flat areas are accessible, the drilled core should be taken 90 degrees on the surface. As two core samples are needed for each shear test, the core samples should be taken pairwise with the two corresponding samples next to each other. To gain trustworthy results, at least four shear tests should be carried out, preferably more. This means that the number of necessary core samples is eight or more.

The samples are then cut, using special rock saws, into approximately 100x100x100 mm cubes, with the original surface roughness still intact. Additionally, the samples should be pairwise surface grinded, so the saw-cut sides of both corresponding cubes are identical and their top sections aligned.

Formwork are then built **afterwards** and adjusted to fit the size of the rock samples. The two corresponding samples should be placed as shown in figure 4.3, with the natural surfaces facing each other. In order for the load plate to fit all of the test-specimens, the distance between the rock cubes should be as close to 100 mm as possible. The formwork should be made out of plywood or a similar material giving a smooth surface.

The two rock surfaces in contact with the concrete should be adequately rinsed, removing all potential sand and dust particles. Concrete with mixture equal to the dam of interest are then cast in between the samples. If the mixture design for the dam is lacking, typical mixture designs for dams built in the same decade should be used. After the concrete is poured, measures should be taken to level the top section of the concrete with the corresponding rock surfaces. The test specimen should then be left to cure at constant room temperature. In order to achieve sufficient compressive strength, the concrete should be allowed to cure for at least seven days.

4.4.3 Testing of Shear Strength

The shear capacity of the test specimen are tested by applying a driving force on the concrete part while both the rock parts are supported and held still on the opposite side. A theoretical setup of the shear tests can be seen in figure 4.14.

.

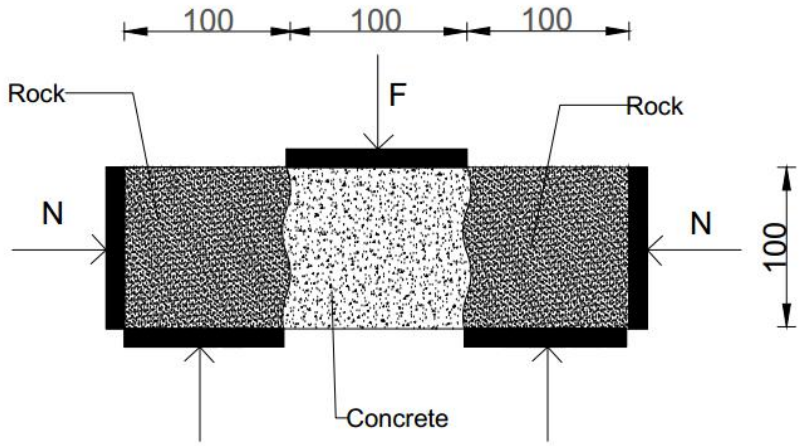

Figure 4.14: Theoretical setup of shear tests.

Both the driving force and the support forces should be equally distributed over the surfaces by using load plates of steel or similar material. To minimize any moment action, the plates should cover the surfaces as completely as possible, while at the same time not overstepping the transition zone between concrete and rock. Clamps can be used to clench the far sides of the rock parts to the steel plates below, as an additional measure to reduce the bending effects

The driving force should be applied on the most even of the concrete surfaces, presumably one of the surfaces that faced the sidewalls of the formwork during the casting process. The test machine should have a minimum capacity of at least 80-100kN, preferably more. Furthermore, the machine should be able to run the tests at a constant shear velocity and log the vertical displacement and driving force continually and accurate. Electromechanical test machines are preferred over the hydraulically driven ones. The reason for this is the somewhat brittle failure mechanism associated with shear failures, which might lead to a small pullback of the loading mechanism for hydraulic machines.

Appropriate normal stress should be applied before the tests are run. The normal load can be applied by mounting two vertical steel plates at both sides of the rock samples, and

connecting the plates using threaded bars and nuts. To measure the normal force, a load cell should be placed in-between the vertical steel plate and the rock at one of the sides. Figure 4.15 shows an example of how the setup of the shear tests can be done.

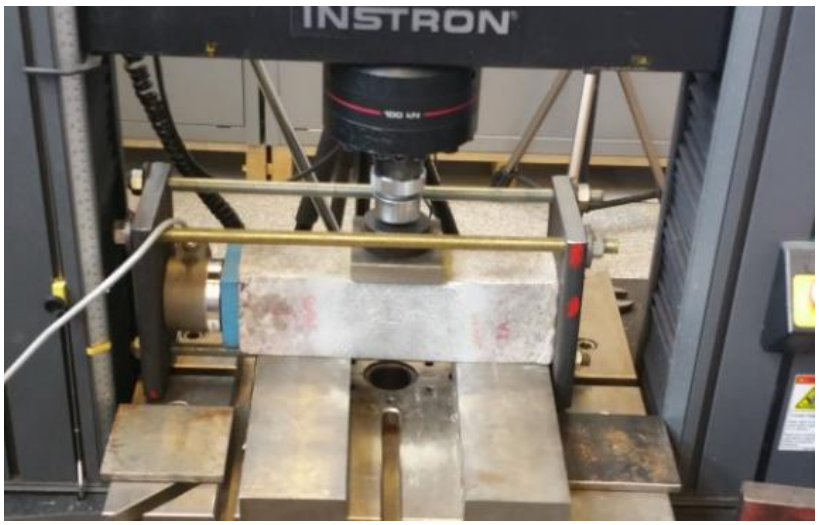

Figure 4.15: Example of setup at testing rig.

Which normal stress levels that is appropriate for the testing depends on the stress levels for the dam of interest. In order to extrapolate out a cohesion value from the test results, the normal stress when the bond fails at peak capacity must vary to some degree. The results from test number I and III from chapter 4.3 indicate that normal stress might remain almost constant until peak capacity of the bond is reached and roughness is mobilized, yet more tests is needed to verify this. Consequently, the preloaded normal stress should be decided from test to test, with the intention of achieving some variance as the bond fails.

The shear test should be run with a consant shear velocity. Typcial shear velocities used in litterature lies in the range of 0.05 to 0.5 mm/min. For the preliminary testing a shear velocity of 0.20 mm/min was used with success.

4.4.4 Interpretation of Test Results

After all the tests have been run, a thorough examination of the test specimen and the gathered test data should be performed. Tests that exhibit anomalous shear behaviour and results, or in any other way fail to represent the actual failure mechanisms of the sliding problem, should be excluded from the analysis.

To estimate the cohesion value, the peak shear stress as the bond is broken and the corresponding normal stress should be found for all the tests. Then by plotting the shear stress against the normal stress for all the cases, and then fitting a linear interpolation function a la Mohr-Coulomb to the data points, the cohesion can be estimated as the point where the interpolation function meet the y-axis and the normal stress is zero. An illustration of how this is done for three hypothetical shear tests is shown in figure 4.16. The average internal friction angle ϕ_i of the concrete-rock contact can also be estimated by simply finding the slope of the interpolation line.

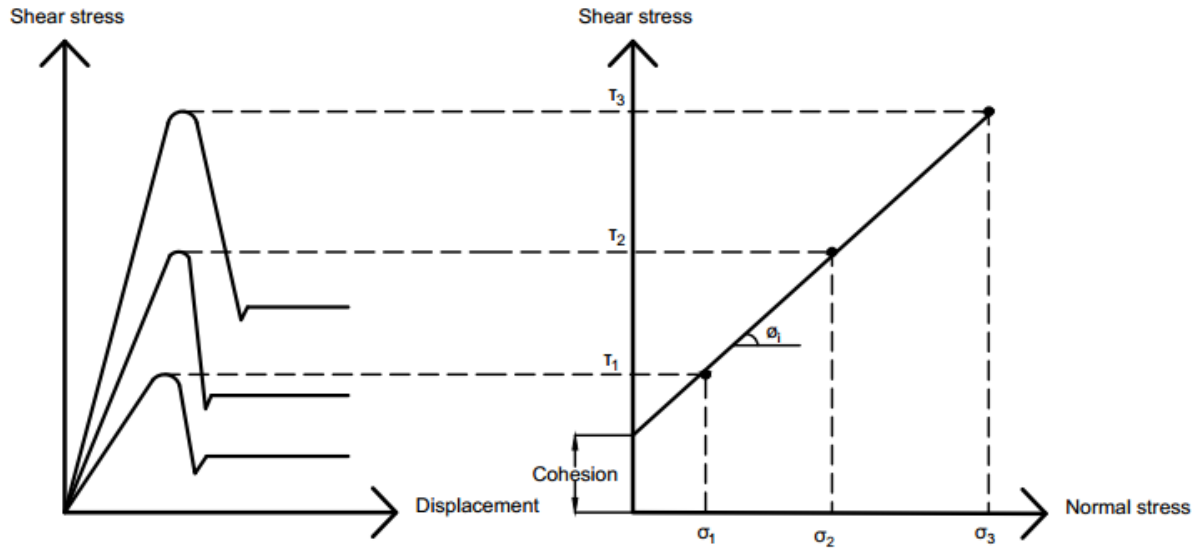

Figure 4.16: Illustration of how the cohesion value can be extrapolated the from test results

4.5 Summary and Discussion

A thorough test methodology for estimating the cohesion between a rock and a concrete surface have been developed and tested. The methodology is based on core samples taken from the dam site, thus taking into account the actual surface roughness and rock strength of the dam foundation. Furthermore, new concrete is cast between the natural surfaces of two rock samples, and three-point shear tests decide the shear capacity. By plotting the shear stress against the normal stress when the bonding fails, the cohesion can be extrapolated through linear regression.

All three test samples from the preliminary testing failed completely or partly in shear in the concrete-rock interface. However, bending action is believed to have contributed significantly on at least two of the tests. It was found that the preparation of the samples is key to precise and trustworthy results. The rock cubes should for instance be pairwise surface grinded and the corresponding couple should be perfectly aligned when put next to each other. This will help to distribute the load evenly, and reduce the introduced bending action. It should be emphasized, however, that removing all bending completely is impossible due to the self-weight of the concrete. Nonetheless, refining the geometry of the test specimen will help minimize the contribution significantly. Ideally, the tests would be run in horizontal shear boxes, but as far as the author knows, there is no shear box affiliated with the research communities at NTNU with high enough capacity to drive bonded concrete-rock specimen to failure. There is a suitable shear box at the Luleå University of Technology (LTU), however, having to transport all the test specimen to the northern part of Sweden for testing is inconvenient as a standardized method of testing cohesion on Norwegian dams.

In order to estimate the cohesion, the normal stress when the bond fails must be known. It is believed that if the test specimen is well prepared and the contribution from bending is minimal, the normal stress will remain practically constant until the peak capacity of the bond is reached and the roughness is mobilized in friction. However, to control that no additional induced normal stress is introduced until bond failure, a continuous logging of the stress is necessary. Furthermore, due to the curvilinear failure envelope of the problem, it is vital that the normal load for the test specimen is in the same range as the expected normal loads of the dam. If the normal stress is too high, fitting a linear Mohr-Coulomb envelope to the test results might exaggerate the actual cohesion and underestimate the friction angle, as illustrated in figure 4.17.

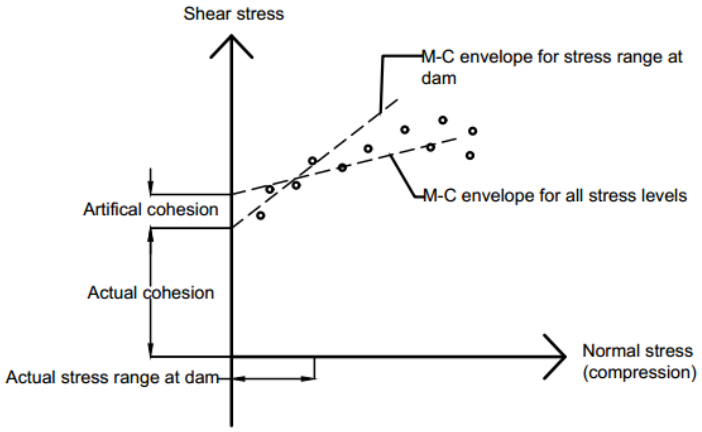

Figure 4.17: Fitting Mohr-Coulomb envelopes to test results using different ranges of normal stress.

One of the weaknesses with the methodology is that the cohesion value found stems from the cementitious bond for new concrete cast on the rock surface, whereas the occurring cohesion between the actual dam and the rock surface remain uncertain. This occurring cohesion is influenced by other factors than the rock quality and roughness alone. For instance, due to the continuous hydration process, a dam will, all else equal, most likely have a higher bond strength than a test-specimen tested with its 7- or 14-day strength. However, leakages and other degradation processes an old dam often experiences might reduce the bond strength (Wilde and Johansson 2013). Furthermore, the cleanness of the rock surface prior to pouring would also have a big impact on the occurring cohesive strength.

In addition, scale effects might be presented when comparing the test results with real sized structures. However, concrete cast on bedrock will, at least in the compressive zone of a dam, have a high degree of matedness (if not perfectly mated). According to the conceptual model introduced by Johansson (2009), the scale effects should therefore be either non-existent or very small.

Nonetheless, it is in the author's belief that the testing procedure will give a good estimate of the expectable cohesive strength of the dam. A lot of the uncertainty concerning the cohesion value is also taken into account by the significantly higher safety factor necessary (2.5 in the Norwegian guidelines). Considering this, it does not seem unreasonable nor unsafe to be allowed to apply a cohesion value obtained from the proposed test methodology to get the sliding stability calculations within NVEs requirements, especially for dams that historically have proven themselves stable.

5. Conclusion

Based on experimental testing, a general method to estimate cohesion in the concrete-rock sliding interface of a flat-slab buttress dam have been proposed. The procedure proposed consists of the following main steps (in chronological order):

- Bonding is verified by core drilling through 10 % of the buttresses of the dam.
- Several core samples of the bedrock at the dam site are taken pairwise.
- The samples are cut into cubes, leaving the original surface intact, and surface grinded to have sides that are perfectly aligned.
- Concrete replicating the concrete of the dam are cast between the natural surfaces of the sample pairs.
- A three-point shear test is carried out to estimate the shear capacity of the concrete-rock interface.
- The value of the cohesion is found by plotting the τ-σ values and examining where the linear regression line meets the τ-axis.

The preliminary testing revealed that the preparation phase is essential for receiving accurate and reliable results. To minimize the introduced bending stress, the rock cubes should have straight and identical sides and measures should be taken to make the concrete surfaces smooth and in alignment with the rock cubes

Some uncertainty exist regarding the cohesive strength of new concrete-rock interfaces versus old ones, that might have experienced weathering and other impairing effects during the years. However, due to the continuous hydration process, the bond strength might as well be greater in old dams, especially if the shear tests are carried out before the 28-day strength is reached for the test-specimen. Nevertheless, by using a higher required safety factor a lot of the uncertainty is accounted for.

It should also be pointed out that even though the methodology primarily have been created with flat-slab buttress dams in mind, with some adjustments it should be applicable to estimate cohesion for other concrete structures cast on bedrock, as for instance concrete gravity dams or bridge abutments.

To investigate the effect of including cohesion in dam stability calculations, the sliding capacity of a flat-slab buttress dam, Kalhovd dam, have also been carried out. The results showed that the dam is unstable against the load combination with highest regulated water

level and ice load. However, by applying reasonable values for the cohesion in the dam in the calculations, it is possible to get the dam within the required safety factors set by NVE.

Additionally, when including cohesion in the calculations, the guidelines from NVE states that the cohesive strength can only be the added to the compressive area of the concrete-rock joint. How this area can be found, though, is not obvious. Using linear elastic beam theory and assuming a linear varying normal stress distribution seemed to overestimate the compressive zone, compared to the stress distribution found from the finite element analysis. Carrying out an FE-analysis is time consuming, however, and the reliability of the results highly depend on the input parameters and assumptions made by the analyst. Ideally, the area of bonded zone is found in-situ using non-destructive testing tools, however, finding suitable tools for this is out of the scope for this thesis.

For future work, the author recommends further testing and development of the test methodology. Additionally, it would be interesting to compare the cohesive strength of old concrete structures cast on bedrock versus the cohesive strength of new concrete cast on the same bedrock. Investigating different non-destructive tools to assess the bonding conditions beneath concrete buttresses could also be very benefitting.

References

Barton, N. (1973). “Review of a new shear-strength criterion for rock joints”. *Engineering Geology*, 7(4), pp.287-332.

Barton, N. and Choubey, V. (1977). “The shear strength of rock joints in theory and practice”. *Rock Mechanics Felsmechanik Mcanique des Roches*, 10(1-2), pp.1-54.

Barton, N. and Bandis S. (1982). “Effects of block size on the shear behaviour of jointed rock”. Proceedings of the 23rd US symposium on rock mechanics, Berkeley, California (1982), pp. 739–760

Barton, N. and Bandis S. (1990). “Review of predictive capabilities of JRC-JCS model in engineering practice”. Proc. Int. Symp on Rock Joints, Loen, Norway, pp 603-610. Rotterdam: Balkema

V.Chaudhari, S. and A. Chakrabarti, M. (2012). “Modeling of Concrete for Nonlinear Analysis using Finite Element Code ABAQUS”. International Journal of Computer Applications, 44(7), pp.14-18.

Dassault Systèmes (2014). “Abaqus Analysis User’s Guide”. Dassault Systèmes Simulia Corp., Proidence, RI, USA.

Donnelly, C.R., Dawson, R. V., Curtis, D.D. (1996). “Sliding Stability of Concrete Gravity Dam”. Canadian Electricity Association, Rehabilitation of Existing Hydroelectric Structures, Hydraulic Power Engineering and Operating Division, Montreal.

Donnelly, C.R. and Rigbey, S.J. (1998). “Concepts of Shear Resistance and Practical Applications”. In: HG Acres Annual Seminar.

Donnelly, C.R. and Rigbey, S.J. (2007). “The Assessment of Sliding Resistance Beneath Concrete Structures”. Conference Paper. Canadian Dam Association Conference, St. John’s, Canada.

Eurocode 2 (2004). “Design of Concrete Structures. Part 1-1: General Rules and Rules for Buildings”. Brussels. 29p.

Electrical Power and Research Institute (EPRI) (1992). “Uplift pressures, shear strengths, and tensile strengths for stability analysis of concrete gravity dams”. Vol. 1. Prepared by Stone and Webster Engineering Corporation, Denver, Colorado.

Geo.ngu.no. (2016). *National Bedrock Database*. [Online] Available at: http://geo.ngu.no/kart/berggrunn/ [Accessed 10 May 2016].

Golder, H. (1948). "Coulomb and Earth Pressure". *Géotechnique*, 1(1), pp.66-71.

Grasselli G. (2001). "Shear Strength of Rock Joints Based on Quantified Surface Description, Ph.D". dissertation, Ecole Polytechnique Fédérale de Lausanne.

Guttormsen O. (2013). «Vassdragsteknikk I». Institutt for vann- og miljøteknikk. NTNU

E. Hognestad (1951). "A study of Combined Bending and Axial Load In Reinforces Concrete Members". University of Illinois. Engineering Experiment Station. Bulletin ; no. 399

Jaeger, J. (1959). "The frictional properties of joints in rock. *Geofisica Pura e Applicata*, 43(1), pp.148-158.

Johansson, F (2009). "Shear Strength of Unfilled and Rough Rock Joints in Sliding Stability Analysis of Concrete Dam"s. PhD. Thesis. Royal Institute of Technology (KTH), Stockholm

Johansson, F. and Stille, H. (2014). "A conceptual model for the peak shear strength of fresh and unweathered rock joints". *International Journal of Rock Mechanics and Mining Sciences*, 69, pp.31-38.

Kosmatka, S. and Wilson, M. (2011)." Design and control of concrete mixtures". Skokie, Ill.: Portland Cement Association. Skokie, Illinois, USA, pp. 260

Krounis, A., Johansson, F. and Larsson, S. (2016). "Shear Strength of Partially Bonded Concrete–Rock Interfaces for Application in Dam Stability Analyse"s. *Rock Mech Rock Eng*.

Ladanyi and Archambault (1969). "Simulation Of Shear Behavior Of A Jointed Rock Mass". The 11th U.S. Symposium on Rock Mechanics (USRMS), 16-19 June, Berkeley, California.

Land and Heck (1964). "Triaxial testing for strength of rock joints". Proc. 6th symp. Rock Mech. Rolla. pp. 98-108.

Mathisen, K., M. (2015). Lecture 7: The Bilinear Rectangle Formulated in terms of Generalized Coordinates, Lecture Note, TKT4192, NTNU, Trondheim, 07. Sept. 2015.

Moradian, Z., Ballivy, G. and Rivard, P. (2011)." Role of adhesive bond on shear mechanism of bonded concrete-rock joints under direct shear test." The 45th US Rock Mechanics / Geotechnics symposium, 26-29 June, San Francisco, California

Moradian, Z., Ballivy, G. and Rivard, P. (2012). "Application of acoustic emission for monitoring shear behavior of bonded concrete–rock joints under direct shear test". *Canadian Journal of Civil Engineering*, 39(8), pp.887-896.

Nicholson, G.A., (1983). "Design of gravity dams on rock foundations: Sliding stability assessment by limit equilibrium analysis and selection of shear strength parameters". Geotechnical Laboratory, U.S. Army Corps of Engineers, Waterways Experiment station

The Norwegian Water and Energy Directory (NVE) (2005). "Retningslinjer for betongdammer". NVE, Oslo.

The Norwegian Water and Energy Directory (NVE) (2012). "Tillegg til retningslinjer for betongdammer", utgave 2 (2005). NVE, Oslo.

Nymo, A. (2015). "Sliding stability of Lightweight Concrete Dams". NTNU, IVM, Trondheim. Unpublished.

Patton F. D. (1966). "Multiple modes of shear failure in rock". Conference paper. 1st ISRM Congress, 25 September-1 October, Lisbon, Portugal

Ruggeri, G. (2004). "Sliding Safety of Existing Gravity Dams – Final Report". ICOLD European Club.

S.A. Miedema., (2014). "The Delft Sand, Clay and Rock Cutting Mode"*l*. IOS Press.

Saiang, D., Malmgren, L. and Nordlund, E. (2005). "Laboratory Tests on Shotcrete-Rock Joints in Direct Shear, Tension and Compression". *Rock Mech. Rock Engng.*, 38(4), pp.275-297.

Statkraft Grøner (2003). "Revurdering av Kalhovd dam og luker Tillegsdokumentasjon". Technical report.

Tian, H. M. , Chen, W. Z. , Yang, D. S. , and Yang, J. P. (2014). "Experimental and numerical analysis of the shear behaviour of cemented concrete-rock joints". *Rock Mech. Rock Engng.* 48(1), pp 213–222

Westberg Wilde, M. and Johansson, F. (2013). "System Reliability of Concrete Dams with Respect to Foundation Stability: Application to a Spillway". *J. Geotech. Geoenviron. Eng.*, pp. 308-319.

Digital Appendix

Files delivered in the digital appendix at daim is:

dam.cae

dam.jnl

Damcalculations.ods

Sheartests.xlsx

Appendix A - Construction drawing from Kalhovd dam

Provided by Statkraft.

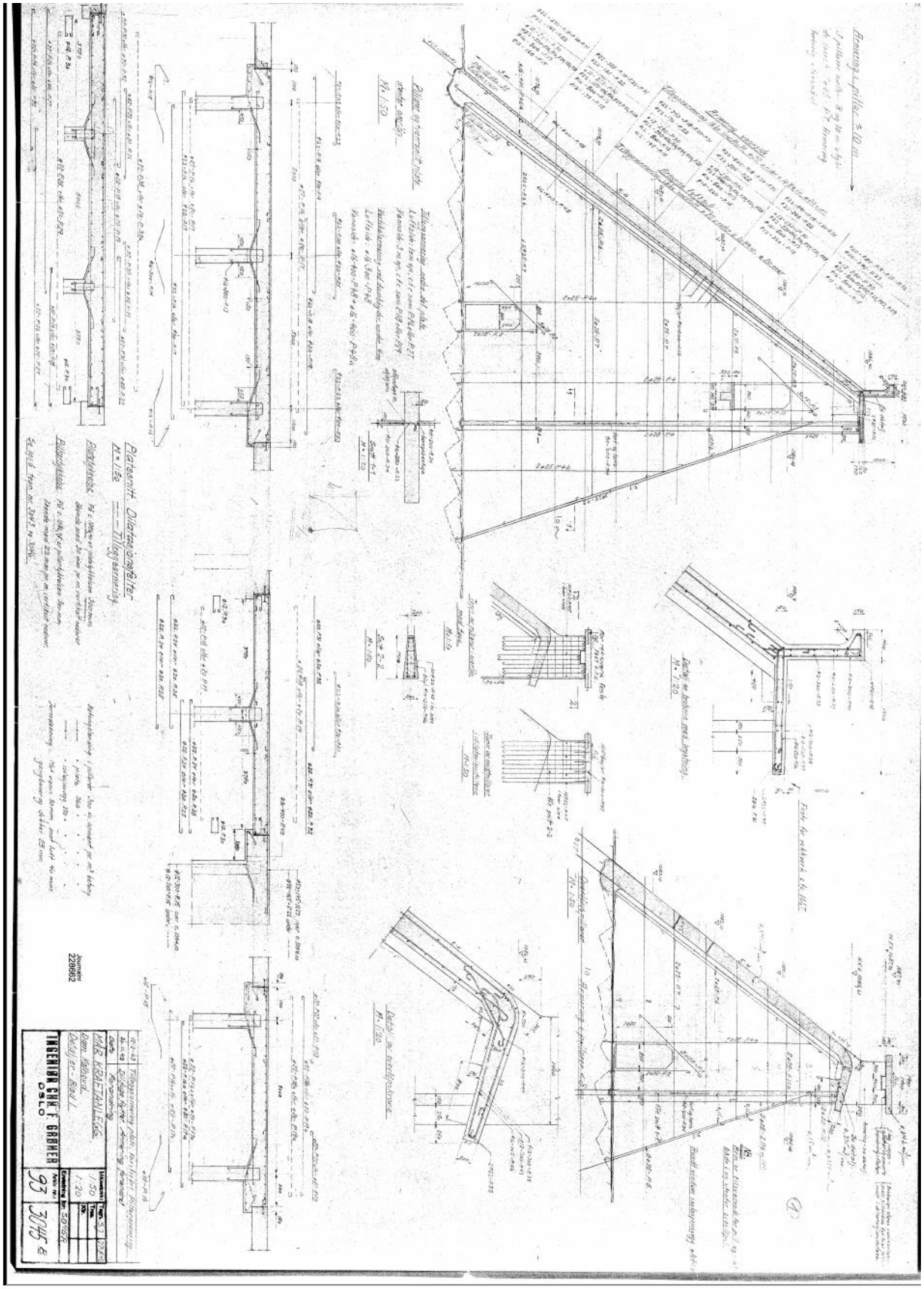

Appendix B – Derivation of safety factor

The safety factor as defined by the shear friction method:

$$FS = \frac{S}{P} \tag{B.1}$$

where *S* is the total shear capacity of the plane and *P* is the total driving horizontal forces.

The shear capacity for a rough rock joint with uplift pressure, according the JRC-JCS model:

$$\tau = \sigma_n' \cdot \tan[JRC \cdot \log_{10}(\frac{JCS}{\sigma_n'}) + \emptyset_r] \tag{B.2}$$

Setting $S = \tau \cdot A$, where A is the total interface area, and $P = \sum H$ gives the following expression for the shear capacity:

$$FS = \frac{A \cdot \sigma_n' \cdot \tan[JRC \cdot \log_{10}(\frac{JCS}{\sigma_n'}) + \emptyset_r]}{\sum H} \tag{B.3}$$

$A \cdot \sigma_n'$ can also be expressed as the sum of the vertical forces $\sum V$, giving the following expression for the factor of safety FS:

$$FS = \frac{\sum V \cdot \tan[JRC \cdot \log_{10}(\frac{JCS}{\sigma_n'}) + \emptyset_r]}{\sum H} \tag{B.4}$$

Appendix C – Photos of test specimen

Side one of test specimen I after failure:

Side two of test specimen I after failure:

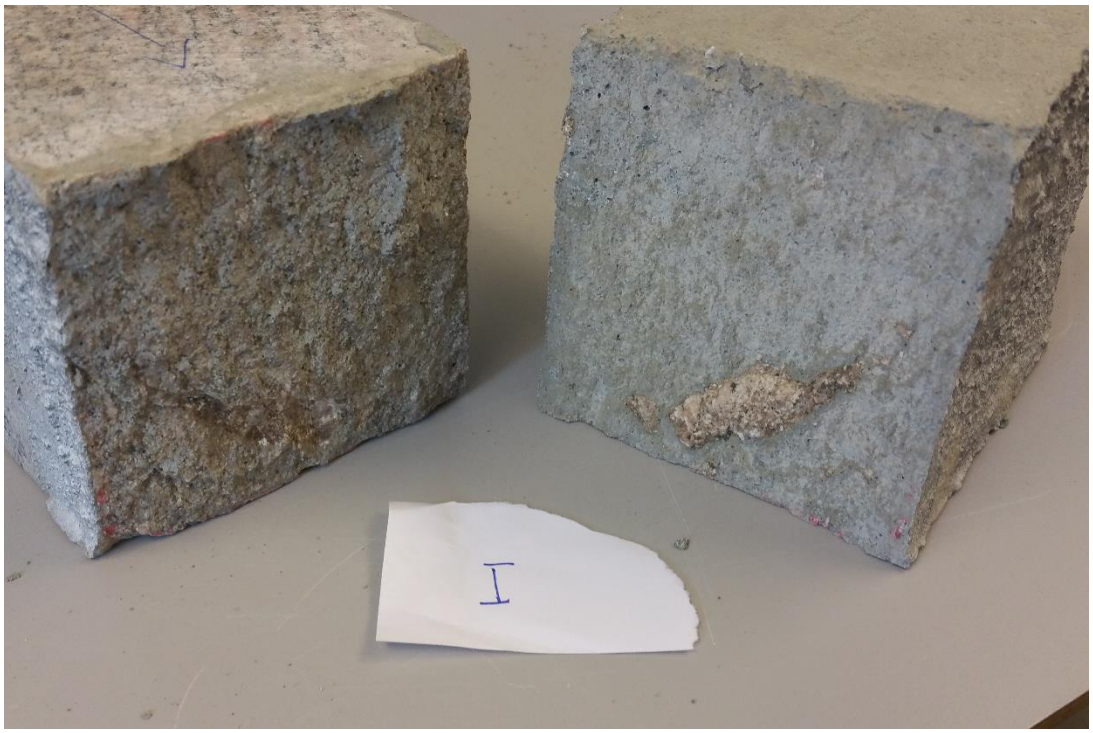

Side one of test specimen II after failure:

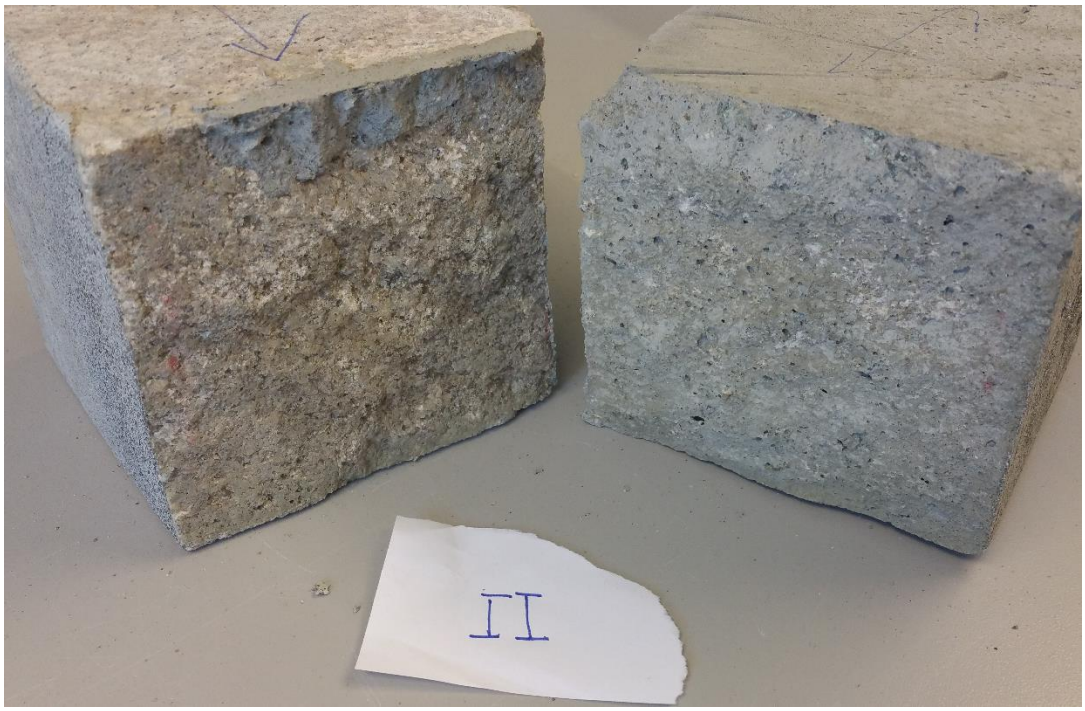

Side two of test specimen II after failure:

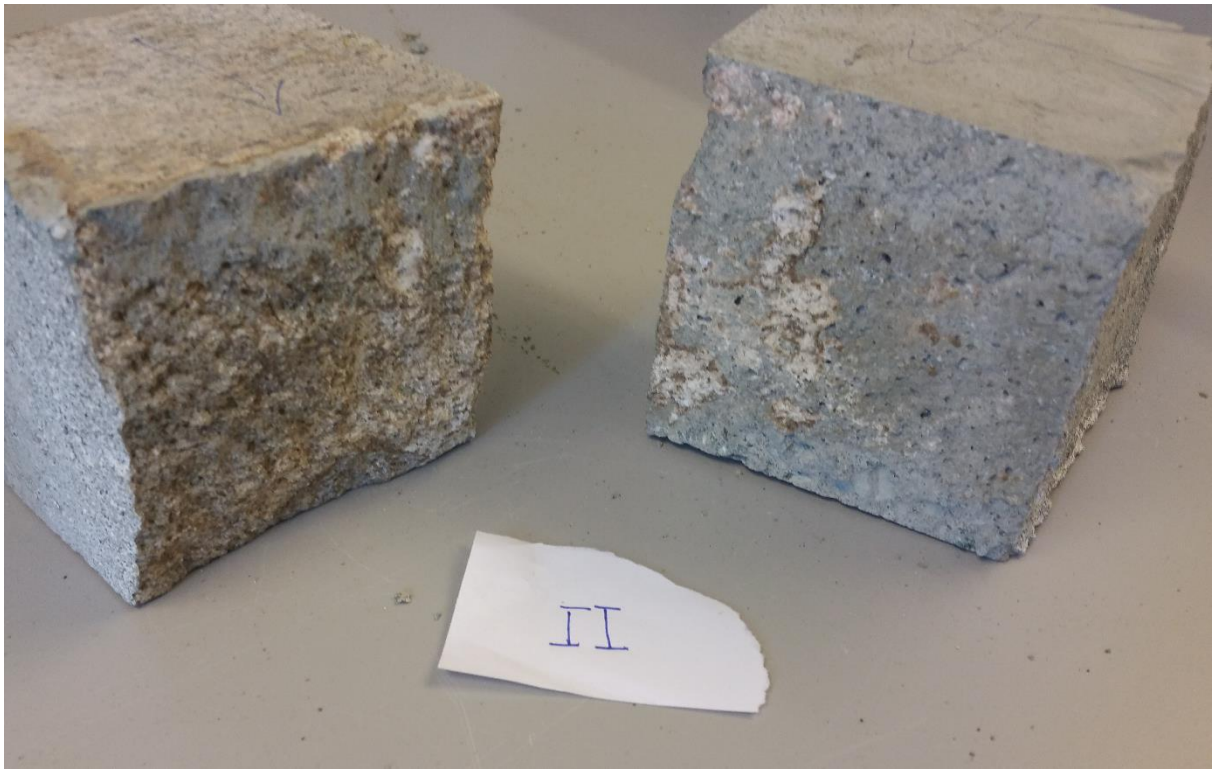

Test specimen III after failure:

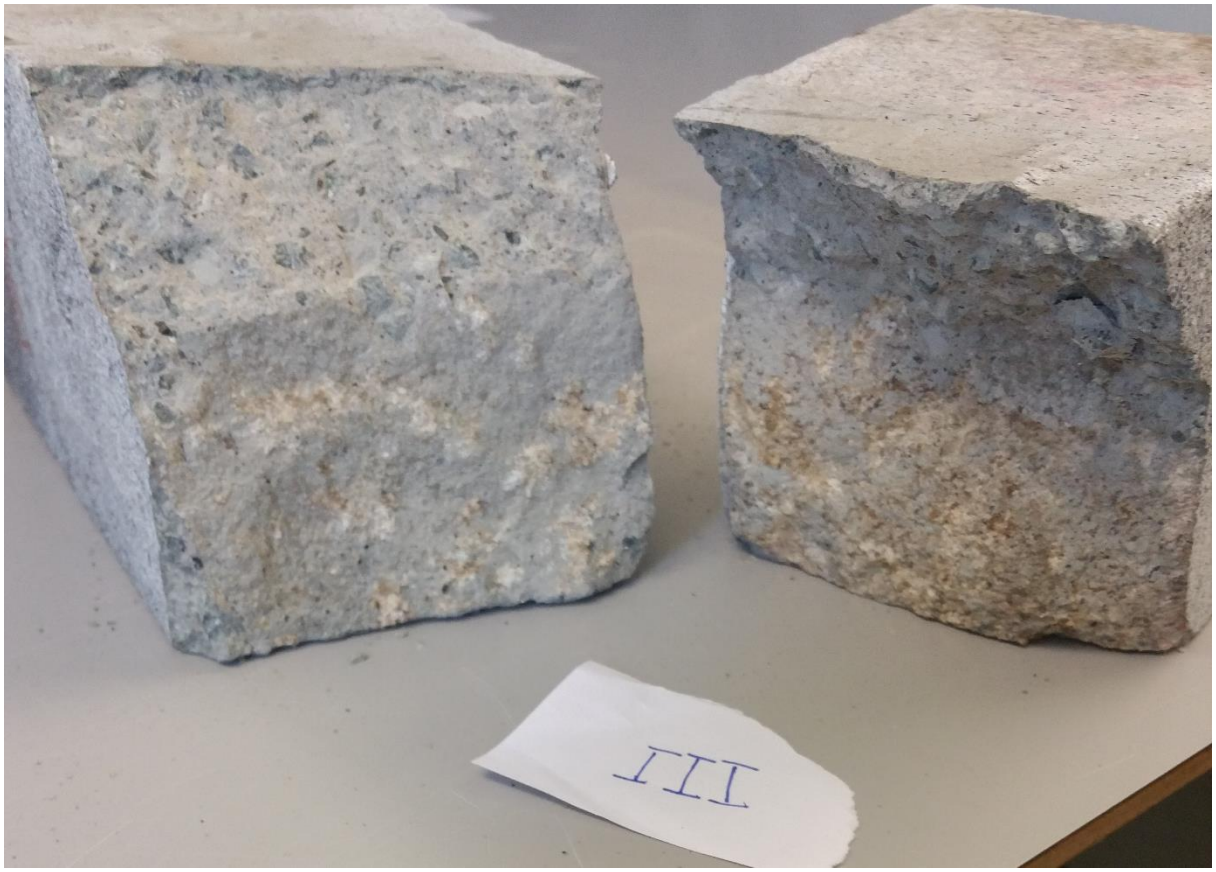

Appendix D – Estimating compressive zone

		V [kN]	a [m]	M [kNm]
Weight damtoe	W1	7.8	0.37	2.93
Weight midsection	W2	37.0	1.31	48.42
Weight frontsection	W3	88.9	2.98	264.72
Weight slab	W4	179.8	3.62	650.88
Weight walkway	W5	96.9	1.31	126.92
Vertical water pressure	Pwv	304.2	4.14	1259.39
Groundwater pressure	Pgw	-87.8	5.40	-473.85
Force rock bolts	Pbolt	353.4	5.40	1908.52
		Vtot [kN]		Mstab [kNm]
	Sum	980.30		3787.92

		H [kN]	a [m]	M [kNm]
Horizontal water pressure	Pwh	380.25	1.3	494.325
Iceload	Pice	500	3.65	1825
		Htot [kN]		Mdriv [kNm]
	Sum	880.25		2319.325

Moment arm	amom	1.50
Length of compression zone	Lcomp = 3*amom	4.49